Development of microelectrodes for electrical measurements in a microfluidic system

Emma Thomée

2017

LUND UNIVERSITY

Master's Thesis in Biomedical Engineering
Faculty of Engineering LTH

Department of Biomedical Engineering

Supervisor: Lars Wallman
Assistant supervisor: Anette Wolff

Abstract

Transendothelial electrical resistance (TEER) measurements are used to quantitatively monitor cell barrier formation in *in vitro* models of the blood-brain barrier. TEER measurements in microfluidic *in vitro* systems are technically problematic and have suffered from poor measurement reproducibility.

The aim of this Master's thesis project was to develop fully integrated electrodes for measuring TEER in a microfluidic blood-brain barrier model. Two patterns of thin film electrodes – one with electrodes placed in the microfluidic channels, and one with electrodes directly above and below the cell culture membrane – were designed, fabricated and embedded in the microfluidic system. Electrodes were fabricated in silver and in platinum, and their reproducibility was evaluated using impedance spectroscopy.

Results showed that electrodes fabricated in platinum and placed directly over the membrane could measure impedance with the highest precision. Measurement variation from the electrodes placed in the channels was shown to effectively be reduced by employing a technique of combining six measurements from four electrodes. Based on the reproducibility studies presented in this report, both types of electrodes were believed to have sufficient sensitivity and robustness to be used for TEER measurements.

A robust technique to measure TEER enables real-time monitoring of cells in microfluidic systems, and offers a quantitative validation parameter for easy comparison and benchmarking of different system.

Acknowledgements

First of all, I wish to thank my supervisor Lars Wallman and assistant supervisor Anette Wolff at the department of biomedical engineering at Lund University. They have both provided invaluable guidance, support and enthusiasm throughout this project. I also wish to thank Martin Bengtsson for teaching me the fabrication processes and assisting during all work carried out in the cleanroom facilities.

At Uppsala University I would like to thank Maria Tenje and the members of the research team EMBLA for welcoming me as a member of the team and for giving me valuable feedback and encouragement. During the project I also got the opportunity to travel to Uppsala to meet with the team and take part of two days of scientific exchange.

Last but not least, many thanks to the staff at Biomedical Engineering for helping and sharing their expertise, as well as for instructing and assisting me in the laboratories.

Table of contents

1. Introduction

By combining the principles of microfluidics, microfabrication and cell culturing techniques, a new type of laboratory platforms has emerged, known as "organs-on-chips". Organs-on-chip systems are microengineered devices containing living cells. Their purpose is to model structure and behaviour of human organs [1]. Among other applications, these systems can be used as screening platforms in the pharmaceutical industry, providing an alternative to animal testing [2]. They have the potential advantage of being easy and cheap to manufacture in large scale while avoiding the ethical issues associated with the use of laboratory animals.

One type of biological structure that has been modelled on a microfluidic chip is the blood-brain barrier (BBB). Previous studies have shown that microfluidic models of the BBB can provide more realistic microenvironments compared to earlier *in vitro* models [3]. A BBB-on-chip is typically made up of two-layered crossing microchannels with endothelial cells cultured on a permeable membrane. These systems show great potential in proof-of-concept studies, but a remaining challenge in the field is the lack of standardisation when measuring quantification parameters [4]. This makes it difficult to compare and benchmark models to other existing models.

The most used parameter to quantitatively evaluate barrier quality in BBB-models is *transendothelial electrical resistance*, commonly shortened TEER. TEER is a measurement of how much the cellular barrier impedes an applied electrical current, which relates to the quality of the barrier. The concept of TEER is simple and well defined. However, there is inconsistency in the measurement procedure and setup. This has been identified as a contributing factor to the large measurement variability of TEER that has been reported in literature [5].

This Master thesis project aims to develop a robust measurement technique to measure TEER in a BBB-on-chip system. Electrodes were developed and integrated in the device, and evaluated by impedance spectroscopy measurements. The report describes and discusses the processes and results of designing, fabricating and characterising the electrodes.

2. Project background and research questions

This master thesis project is a collaboration with an on-going research project aiming to develop a BBB-on-chip model. The principal goal of this thesis is to develop integrated electrodes for measuring TEER. Electrodes are primarily developed to be integrated in this device, but with the ambition to also be implementable in other two-layered channel systems separated by a membrane. This project sets out to be a first experimental study about electrical measurements on the device, laying the groundwork for future studies. The resulting components aim to be used in research.

The following research questions constitute the framework of the project:

1. Can integrated electrodes provide stable and reproducible impedance measurements?
2. How can the electrode design and measurement set-up be optimised to reduce measurement related variations?
3. Can the integrated electrodes be used to measure TEER in a microfluidic BBB-model?

The device, which has been developed at the department of biomedical engineering at Lund University, is made up of two layers of polydimethylsiloxane (PDMS), each comprising a 500 μm high channel. Where the two channels overlap, a thin, permeable membrane for endothelial cell seeding is embedded, allowing diffusion between the channels through the membrane and the monolayer of cells. Free diffusion is assumed across the membrane. The PDMS layers are positioned between two layers of glass. Each channel has a fluid inlet/outlet connected form the top of the chip. The device is expected to hold flow rates around 920 mL/h, corresponding to the flow needed to reach physiological sheer stresses [6]. An illustration of the chip at the start of the project is presented in figure 2.1.

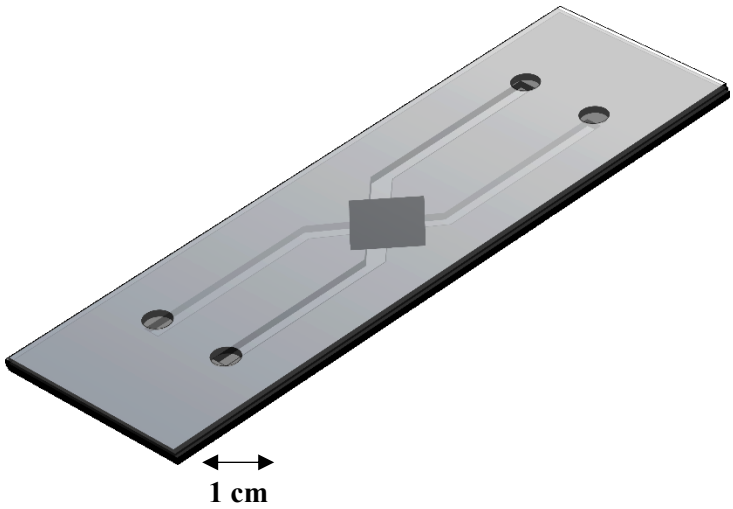

Figure 2.1: Illustration of the BBB-on-chip model at the start of the project.

3. Theoretical Background

This chapter summarises the theoretical background information that the project is based on. The biology of the human BBB is shortly presented, followed by a description of BBB *in vitro* models and TEER measurements. The final sections discuss electrical impedance spectroscopy and microfabrication techniques that were used in the project.

3.1 The blood-brain barrier

The BBB is the boundary layer of specialised endothelial cells that separates blood from brain interstitial fluids. They make up the blood vessels in the brain. The endothelial cells of the BBB are surrounded by a basement membrane and four other types of cells: astrocytes, pericytes, neurons and microglia. These five types of cells and the basement membrane together make up the neurovascular unit (figure 3.1) [7].

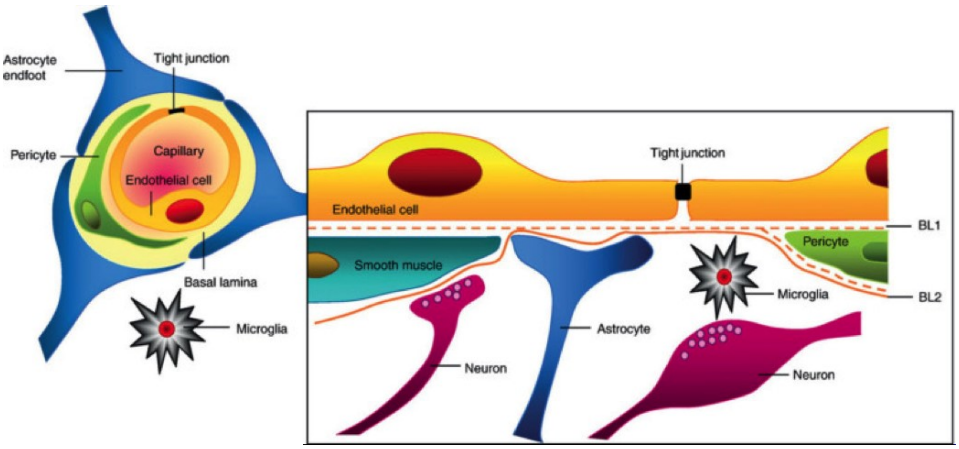

Figure 3.1: A schematic image of the neurovascular unit, showing its five types of cells [7].

The main function of the BBB is to act as a physical and metabolic barrier by allowing selective transport of nutrients through, but preventing toxic substances in the blood from entering the brain. There are two main pathways for transport across the BBB (figure 3.2) [8]:

1) the transcellular pathway
2) the paracellular pathway.

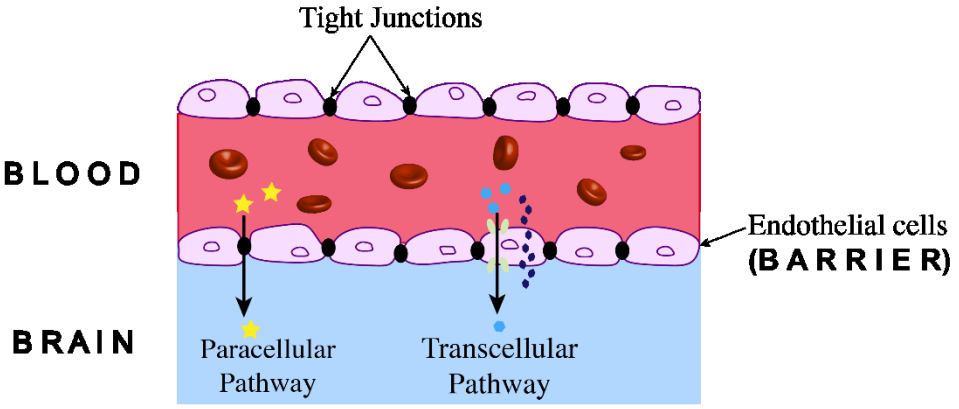

Figure 3.2: A schematic image of the BBB, showing the paths of transport across the barrier.

The specialised endothelial cells differ from normal endothelial cells as they are positioned very close to each other. Sealing protein complexes called tight junctions are formed between adjacent cells. As a result, cells are held in close proximity to each other, thereby occluding the intracellular spaces and preventing transport through the paracellular pathway. Transport across the transcellular pathways is regulated by transport proteins which is very selective, only allowing specific substances to cross. Small molecules, such as oxygen and carbon dioxide, can passively diffuse across the BBB [8].

This high barrier tightness is characteristic of the BBB, and crucial for maintaining brain homeostasis. A local disruption of tight junctions, disrupting the barrier tightness resulting in a leakage through the BBB, is associated with several diseases of the central nervous system (CNS) [9]. Understanding and overcoming the BBB is essential for treatment of diseases on the CNS. Drug delivery systems that can temporarily open the barrier, allowing medication to pass through and reach the brain, is a key research area for the treatment of CNS diseases.

3.2 BBB *In vitro*

In vivo studies of the whole brain performed on laboratory animals have provided useful information about the BBB. The main advantage of *in vivo* models in the form of laboratory animals is that the brain can be studied in its natural, complex environment [10]. However, due to ethical issues and poor conformance to the human brain, research has put effort into mimicking the human brain environment *in vitro,* based on cell culture techniques [11]. In artificial environments conditions can be kept under high control and specific behaviours can be independently studied with little interference of other factors. *In vitro* models can be produced at low cost and can therefore be used for high throughput experiments. Traditionally, the BBB has been reconstructed *in vitro* as two-dimensional, static models. However, microfluidic organs-on-chip models are now progressing as an applicable alternative [12].

3.2.1 Validation of in vitro models

Essential questions when developing BBB *in vitro* models are: "How do we know that the model is a good representation of the physiological BBB?" and "How can we ensure that the barrier is tight enough to study the permeability of different substances?". There are several methods to validate the barrier tightness of BBB models. No one technique alone is good enough to characterise the barrier tightness, but combining several qualitative and quantitative measurements can give a good indication. Commonly used qualitative validation methods include fluorescence microscopy and western blot. The most used quantitative parameters for validation are permeability measurements of solutes and TEER measurements. Although most microfluidic BBB models have been evaluated by measuring the TEER, far from all models have [12]. Possibly, TEER measurements are excluded from some studies due to uncertainties around how to properly measure it.

3.2.2 The next generation of in vitro models: organs-on-chips

Recently, BBB models based on organs-on-chip technology have become a prominent class of *in vitro* models. BBB-on-chip models show several advantages over the traditional two-dimensional, static models. The static BBB models, such as the popular and commercially available Transwell cell culture insert (Corning Inc., Corning, NY), consists of a membrane suspended in a well of cell culture medium where endothelial cells are usually grown on top of the membrane (figure 3.3). Although these models are fit for many types of cell studies, they are often too simple and fail to replicate parts the physiological environment [3]. Organs-

on-chips however, can be designed with more realistic architectures. Their small dimensions better represent the geometry of the capillaries in the neurovascular unit. Bringing cell cultures down to the microscale minimises the number of cells needed, resulting in lower operation costs. Further, by employing microfluidics instead of conducting experiments in a bulk solution, the models can display physiological phenomena such as fluid flows and shear stresses. Another advantage of BBB-on-chip models is that sensors for real-time monitoring can be integrated [2].

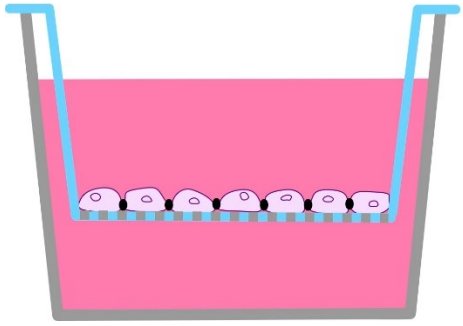

Figure 3.3 Illustration of a Transwell cell culture insert. A monolayer of endothelial cells are cultured on top of a membrane.

3.3 Transendothelial electrical resistance

TEER describes the resistance across a cellular barrier, and is often used as a validation tool to control if endothelial cells in BBB models form tight junction complexes [4]. If the endothelial cells are growing properly and form tight junctions to adjacent cells, the intercellular spaces of the cell layer are occluded and the flow of current through is restricted [13]. This induces a higher resistance to current, which is reflected in higher TEER values. TEER is often expressed normalised to the membrane area in the unit Ωcm^2, as in *formula 1* below, to facilitate direct comparison to other models.

$$TEER\ (\Omega\ cm^2) = Resistance\ (\Omega) \times Cell\ culture\ area\ (cm^2) \qquad (1)$$

The concept of TEER was first introduced by Crone et al. in 1982 [14], when they measured the voltage drop along frog vessels. In BBB models, measuring TEER

is a quick, non-invasive method enabling real-time evaluation of the quality of the barrier. The measurements are performed by applying a low electrical current across the cellular layer, while measuring how much the current is impeded by the cell layer.

3.3.1 TEER measurements in vivo

TEER measurements have been performed *in vivo* in frogs and rats, with a derived average TEER of 1840 Ωcm^2 [14] and 1500 Ωcm^2 [15] respectively. The same measurements performed in mesenteric capillaries, on cells that do not from tight junctions, gave TEER results in the range of 1-3 Ω cm^2 [14]. This significant difference in TEER between cells that form tight junctions and cells that do not from tight junctions, demonstrates the effectiveness of TEER as a method of monitoring tight junction formation. Due to ethical reasons, these measurements have not been performed on the human body, and the specific TEER values of the human BBB are thus unknown.

3.3.2 TEER measurements in vitro

TEER measurements are performed on both static and microfluidic BBB *in vitro* models. In static models, TEER can be measured by inserting chopstick electrodes to both sides of the membrane and measure resistance before and after the cells form tight junctions. The resistance measured before makes up the baseline of the system, and is subtracted from the resistance measured after, in order to isolate the TEER value that is caused by the formation of tight junctions. Although there are well-established measurement protocols for this type of measurement in static models, there are limitations to both the measurement setup and the biological relevance of the results. Static models fail to recapitulate the biological feature of fluid flow. As there is no fluid flow present, the cells are not exposed to shear stresses, which is expected to influence the cell differentiation and enhance the formation of tight junctions [16]. Regarding the measurement setup, chopstick electrodes are criticised for uneven distribution of current flow, especially in large chambers [17]. Further, the measurements are vulnerable to movement of the chopstick electrodes which makes it difficult to repeat measurements, causing large variances between measurements. Alternatively TEER can be measured with commercially available systems specifically developed to measure TEER, such as Endohm cups (WPI inc), Millicell® inserts (EMD Millipore) and the CellZscope® (NanoAnalytics) system.

TEER measurements are also challenging to perform in microfluidic models. Due to their small geometries, chopstick electrodes are too large to fit inside the systems. The commercially available TEER measurement systems previously

mentioned are primarily developed for the Transwell insert and not compatible with microfluidic models. These systems can therefore not measure TEER of microfluidic models *in situ,* and thereby only give indirect estimations of the TEER in the device. Recently, efforts have been made to integrate electrodes in the microfluidic device to measure TEER *in situ* [18] [19]. A summary of TEER values in literature measured by integrated electrodes is presented in table 3.1.

Article/Reference	**Cell type**	**Methods**	**TEER (Ωcm^2)**
Henry et al. (2017) *[19]*	hAECs	Gold thin film electrodes 4-point configuration, impedance spectroscopy	121 ± 6 (± SEM)
van der Helm et al. (2016) *[20]*	hCMEC/d3	Platinum wire electrodes in channels 2-point configuration, multiple paths impedance spectroscopy	22 ± 1.3 (± SEM)
Griep et al. (2013) *[21]*	hCMEC/d3	Platinum wire electrodes 2-point configuration, impedance spectroscopy	36.9 ± 0.9 (± SEM)
Booth et al. (2014) *[18]*	bEnd.3	Ag/AgCl thin film electrodes 4- point configuration, resistance measurements	223
Douville et al. (2010) *[22]*	bEnd.3	Ag/AgCl electrodes 2-point configuration, impedance spectroscopy	≈150-200
Wang et al. (2016) *[17]*	BMECs in monoculture and coculture	Ag/AgCl electrodes 4-point configuration, resistance measurements	Monoculture: 368 ± 60 (± SD) Coculture: > 2000

Table 3.1 Summary of TEER values measured from integrated electrodes reported in literature

Like in the static models, TEER measurements in microfluidic models have suffered from measurement variabilities and low sensitivity. It has been pointed out that TEER measured in microfluidic models differ from TEER measured in Transwell models using the same cell line [5]. It remains a challenge to produce stable TEER results that can be reproduced in a robust manner. A prominent source of measurement variability appears in microfluidic models with long and narrow channels. This is because the resistance of the medium in the channels is often in the same order of magnitude as, or higher than, the resistance across the cell layer. Medium inhomogeneity, due to change in temperature or concentration, affects the resistivity and can thus significantly affect the TEER readout [20]. Additionally, as a consequence of the high channel resistance, small movements of electrodes may cause a relatively large change in total measured resistance of the system. However, many sources of variation can be eliminated with a robust measurement setup [5].

In vitro models of the BBB need to reach TEER values above 150-200 Ωcm^2 to be considered acceptable models [23]. This is approximately a factor ten lower than the reported *in vivo* results. The reason why a much lower TEER is accepted is due to the simplified conditions *in vitro*. An *in vitro* model does not recapitulate all features of the biological blood-brain barrier, and the formation of tight junctions is therefore less effective. Furthermore, it is difficult to avoid short circuit paths for the current as a consequence of small gaps in the monolayer, resulting in lower TEER [9].

3.4 Impedance Spectroscopy

The electrical impedance, Z, is defined as the complex ratio between potential difference and current in the frequency domain [24]. It can be understood as the opposition to flow a current of charged particles experiences in a circuit when an alternating voltage is applied. Introducing the concept of impedance extends Ohm's law to include AC circuits, also taking phase differences into account. Impedance is a complex quantity and can be presented in the form:

$$Z = R + jX, \quad (2)$$

where the real term, R, is the resistance and the complex term, X, is the reactance. The impedance magnitude, $|Z|$, is the ratio between voltage difference amplitude and current amplitude and the argument, θ, represents the phase difference between the voltage and current. A graphical demonstration of impedance is illustrated in figure 3.4.

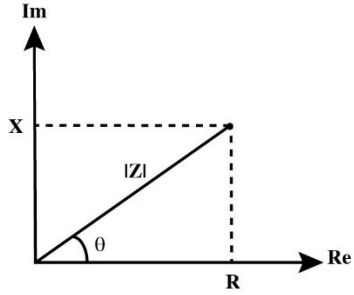

Figure 3.4: A graphical illustration of the concept of impedance.

Electrical impedance spectroscopy is a powerful analytical technique used to measure impedance. It can be applied to characterise electrical properties and behaviour of electrodes and electrolyte materials, including living cells. Real and imaginary impedance can be measured at different frequencies under an applied current and potential. Impedance magnitude and phase shift is presented as a function of frequency.

3.4.1 Electrical impedance spectroscopy for TEER measurements

Instead of measuring TEER as an ohmic resistance by conventional DC resistance measurements, a more reliable technique based on impedance spectroscopy is generally preferred [25]. In addition to not harming the cells and electrodes like a DC current, impedance measurements performed over a range of frequencies has the advantage of characterising the frequency dependent components of the cells, such as the electrical capacitance of the cellular membrane. To derive TEER from impedance measurements, an equivalent electrical circuit diagram must be constructed. From the impedance spectra, individual parameters of the cell layer can be derived by equivalent circuit modelling [26]. Curve fitting algorithms, such as least square algorithms, can subsequently be applied to fit the model to the experimental data. How the circuit should be composed depends on the measurement setup and electrode configuration. A general approach to equivalent circuit modelling is to use the minimum number of elements that can describe the details of the system [27]. A complex model can provide a very good agreement to the data but at the risk of losing the physiological relevance of the individual elements. Several different models can provide equally good fits. In such cases, additional independent experiments may be needed to further characterise the system in order to identify the most relevant model.

For BBB models, applied current passing through the cellular layer can either take the paracellular pathway between cells or the transcellular pathway through the cells. In an electrical circuit model, the paracellular pathway can be modelled as

a single resistance. This resistance is experienced because of the tight junctions, and is known as the TEER. The transcellular pathway can be represented by a resistor and a capacitor in parallel, as the phospholipid bilayer of the cellular membrane has a capacitive effect [25]. Together, these elements make up the total impedance exerted by the cell layer. Additionally, when measuring TEER from integrated electrodes in microfluidic devices, the contribution of system parameters to the total impedance must also be considered. System parameters include resistance of the cell culture medium and the capacitance of the electrodes. An electrical circuit describing the impedance of a BBB model is presented in figure 3.5.

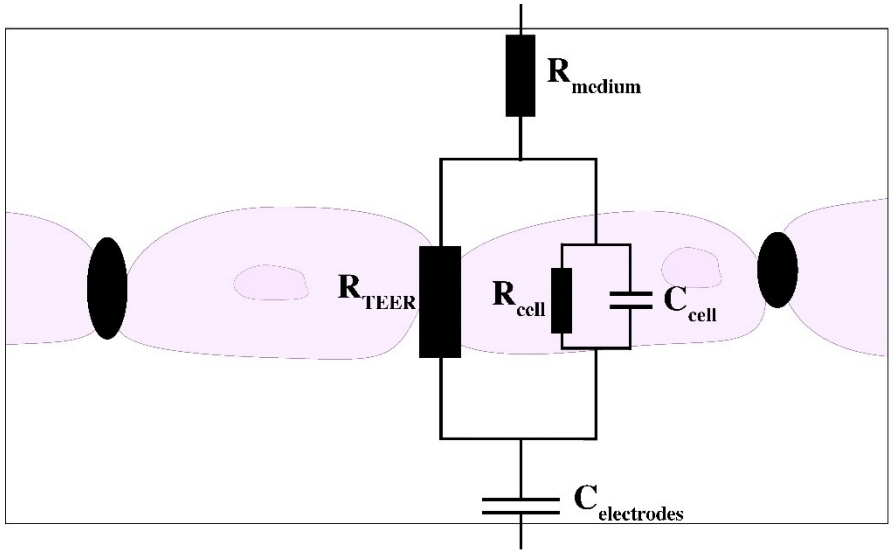

Figure 3.5: An electrical circuit describing the impedance of a BBB model, adapted from Benson et al. [25].

3.5 Microfabrication

There are many advantages of taking electrode fabrication down to the microscale. Miniaturising chamber dimensions makes diffusion times for ions to reach the electrodes faster, resulting in a faster response. Miniaturisation of components also reduce the amount of material and reagents needed, making the fabrication and measurements cheaper in large scale [28]. This chapter discusses the electrode materials and fabrication techniques that were used in this project.

3.5.1 Electrode properties

For good biocompatibility and conductivity, electrical measurements in systems containing living cells are usually performed using gold, silver/silver chloride (Ag/AgCl) or platinum electrodes. Gold and platinum are chemically inert electrodes that do not participate in a chemical reaction with the electrolyte. Silver is more reactive, but is available at lower costs and has better conductive properties. The Ag/AgCl electrode is a non-polarisable redox electrode. The overall electrochemical reaction for Ag/AgCl electrodes can be written as:

$$AgCl_{(s)} + e^{-} \rightleftharpoons Ag_{(s)} + Cl^{-}_{(aq)} \qquad (3)$$

Impedance measurements over cell monolayers have mainly been performed using a two-electrode configuration [22], but also using a four-electrode configuration [19]. In a two-electrode configuration voltage is applied between the same electrodes as the current, whereas in a four-electrode configuration the voltage is separated from the current path. Separating the current and the voltage has the advantage of excluding system parameters related to the double layer capacitance of the electrodes. A double layer capacitance occurs as ions in the electrolyte adsorb to the electrodes, resulting in an ionic double layer acting as an electrical capacitor. This effect is frequency dependent and occurs at low frequencies [29]. The choice of electrode configuration depends on the measured circuit, magnitude of impedance and frequency range.

3.5.2 Electrode fabrication techniques

Photolithography is the process of transferring a pattern onto a wafer by optical techniques. It is generally the first step in a microfabrication process. The photolithography process involves the following principal steps: photoresist coating of water, selective UV exposure through a photo mask, developing to obtain the photoresist pattern [30].
Firstly, photoresist is spun onto a wafer, forming a thin, uniform layer on the wafer surface. The photoresist solution contains a light-sensitive component and a polymer. A negative photoresist polymerises when exposed to light, causing it to be insoluble to the developer solution. A positive resist, on the contrary, becomes soluble when exposed to light. By selectively exposing the resist to UV-light through a photo mask, the desired pattern of the mask is transferred to the wafer. When placed in a developer solution, the soluble parts of the resist layer dissolve, leaving a pattern of resist on the wafer. The photoresist pattern can serve as a mask in microfabrication processes such as etching, moulding and lift-off.

“Lift-off” deposition is an additive microfabrication technique, where a layer is deposited on top of a sacrificial layer [30]. The sacrificial layer is commonly a photoresist pattern, and the deposited layer can be a thin film layer of metal. The wafer is then placed in a developer solution that removes the resist, thereby “lifting off” the unwanted parts of the deposited layer, leaving only the parts that were deposited directly onto the wafer. Multiple layers can be deposited on top of each other using this technique. There are several processes by which a layer can be deposited onto a wafer. In evaporation deposition, the source material is evaporated in a vacuum. The evaporated particles travel freely in the vacuum until they reach the surface of the target material, where they condense back to solid state. Another technique is electron beam sputtering, where an electron gun scans a focused beam of electrons over the wafer surface [30].

4. Method

This chapter describes the methodology and materials of the project. Although the method is presented in a chronological order, the work process was mainly iterative rather than linear. The methods that constitute this project are: a literature study, design of electrodes, fabrication of electrodes and impedance experiments. The electrode designs that were created, were motivated by observations from the literature study. The main factor that was of interest in this study was the placement of the electrodes.

4.1 Literature study

A literature study was carried out to gain essential background information about TEER measurements, impedance spectroscopy and microelectrodes. The literature study also aimed to collect information needed to select a main approach and procedure on how to measure TEER. The search tool *LUB-search* from Lund University libraries was used to search for relevant scientific papers. Search keywords included: blood-brain barrier; TEER; transendothelial (/epithelial) resistance; organs-on-chips; impedance spectroscopy. 22 scientific papers were selected to be studied extensively.

4.2 Electrode design

Two different thin film electrodes patterns were designed, named square electrodes and ring electrodes (figure 4.1). The two-dimensional drawings were made using the software AutoCAD (Autodesk). Each chip had four electrodes, two on the top glass above the membrane and two on the bottom glass, below the membrane. The square electrodes were patterned to be placed in the four microfluidic channels, and the ring electrodes were placed directly above and below the cell culture membrane. The same drawing was used for both the top and the bottom electrodes.
Electrode pads were made for easy electrical connections. The electrode pattern was designed to fit onto standard-sized microscope slides, allowing the device to be studied under microscope. Support lines to facilitate the alignment of the layers were also patterned. Electrodes were fabricated in silver and platinum, and the suitability and performance of the two metals were compared. As neither of the metals adheres well to glass, an adhesive layer of titanium was first deposited. All

four electrodes on a chip were designed to have exactly the same surface area. The square electrodes and the ring electrodes had surface areas of 7.5 mm^2 and 1.1 mm^2 respectively.

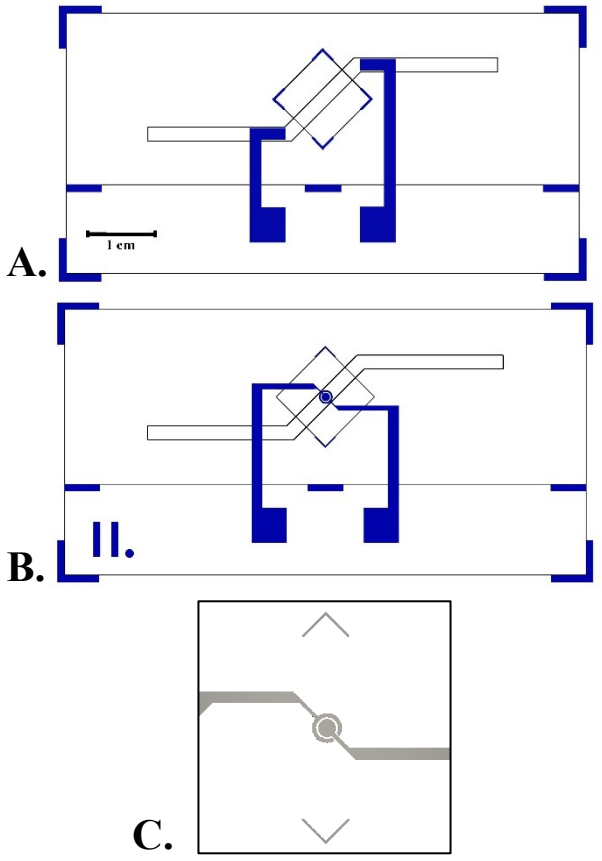

Figure 4.1: Drawing of the two electrode designs, adapted from the CAD-drawings, (A) square electrodes, (B) ring electrodes (with enlargement of the sensing structures, (C)).The coloured parts represent the metal structures that were to be patterned on the glass.

4.3 Fabrication

Thin film electrodes were fabricated on microscopic glass slides that make up the outermost layer of the device. The fabrication process was carried out in a clean room.

4.3.1 Fabrication of electrodes with photolithography

The metal electrodes were deposited onto 75*38 mm glass microscope slides using UV lithography techniques. The fabrication steps are illustrated in figure 4.2. Firstly, a photo mask with the pattern of the electrode design was fabricated. The CAD-files were used as templates to print the patterns on a 100*100 mm chromium wafer by a mask writer instrument (DWL66, Heidelberg Instruments). The photo mask was developed in diluted Microposit 351 solution and subsequently wet chromium etched (Appendix A.1).
Secondly, a 4 µm layer of negative photoresist (AZ nLOF 2020, AZ Electronic Materials GmbH) was spin coated onto clean microscope slides. An established spin protocol was used (Appendix A.2). The glass slides with photoresist were prebaked on a hotplate to drive off solvent from the photoresist.
The baked wafer was exposed to UV light by placing the wafer in a mask aligner (Karl Suss Mask Aligner MA4) and placing the photo mask directly on top of the wafer. The wafer was exposed for 9 seconds resulting in crosslinking of the resist, and was subsequently post baked for one minute to solidify all the resist. The photoresist was developed using the developer AZ 326 MIF Developer (AZ Electronic Materials), to dissolve the unexposed regions on the wafer (Appendix B.3). Thin layers of titanium and silver or platinum were sputtered on the wafer in a thermal evaporator (Auto 306 Vacuum Coating System, BOC Edwards). Lift-off was performed by submerging the wafer in dimethyl sulfoxide (VWR Chemicals) at 80 ºC (Appendix A.4).

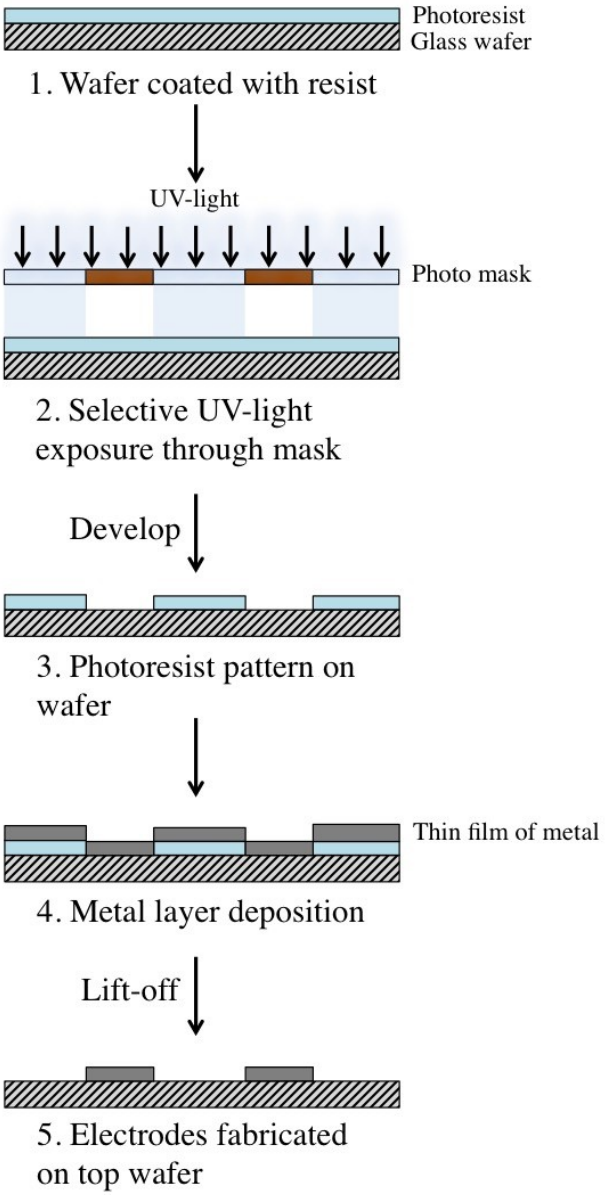

Figure 4.2: A summary of the electrode fabrication steps.

4.3.2 Assembling the device

After having patterned the electrodes to glass slides, the whole 4-layered chip was assembled. 500 µm thick PDMS pieces containing the channel structures were moulded. The whole device, consisting of glass-PDMS-membrane-PDMS-glass, was bonded together using oxygen plasma. After bonding, the assembled chip was left under pressure overnight to form a non-leaking chip. A schematic illustration of the complete chip is presented in figure 4.3 and figure 4.4.

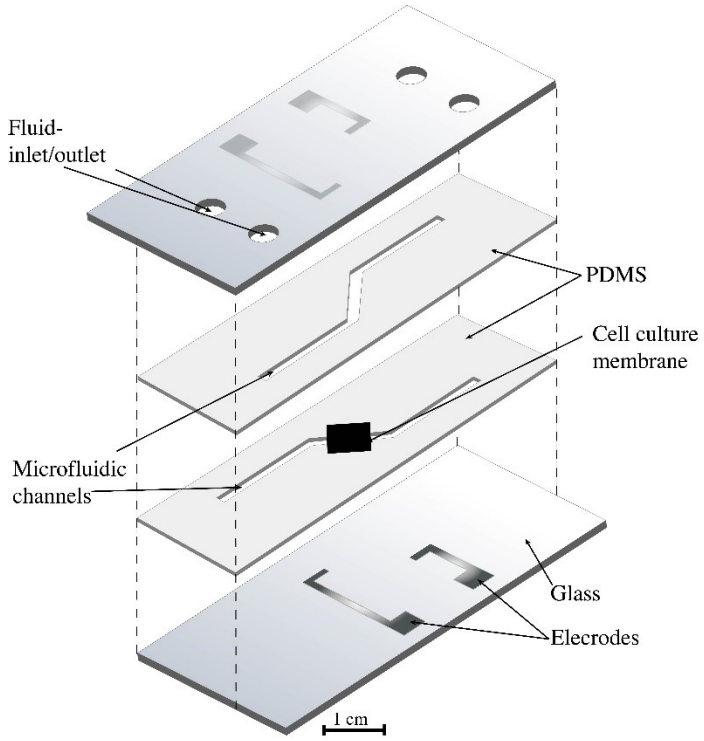

Figure. 4.3: A schematic illustration of the 4 layers and membrane that constitute a complete chip.

4.4 Electrical Impedance Measurements

Electrical impedance measurement setup consisted of an impedance/grain-phase analyser (HP4194A, Hewlett-Packard, Palo Alto, USA) connected with probes to the electrode pads on the chip. The system was controlled by a customised MATLAB®-script. An alternating voltage input signal of amplitude 0.5 V_{RMS} was applied over the frequency range 100 Hz to 1 MHz. By measuring the current, real and imaginary impedance components were derived and presented as impedance magnitude and phase shift. 400 evenly spread data points were recorded per frequency scan. One frequency scan took approximately 5 seconds.

4.4.1 Measurement procedure

All measurements were performed between two electrodes in a 2-point configuration. Channels were filled with modified cell culture medium (DMEM, Sigma Aldrich) prior to measurements. A full measurement protocol was created and is presented in appendix C.

Impedance measurements were performed on:
- 2 single channel prototype devices with two silver square electrodes
- 2 blank (no membrane) chips with silver square electrodes
- 2 blank chips with platinum square electrodes
- 1 chip with membrane and platinum square electrodes
- 1 blank chip with platinum ring electrodes
- 1 chip with membrane and platinum ring electrodes

A picture of a chip during impedance measurements is shown in figure 4.4. The labelling system presented in figure 4.4 was used consistently. At each time of measurement, the impedance between two electrodes (E_i – E_j) was measured for all electrode combinations on a chip, a total of six measurements. To evaluate the robustness of the electrodes, impedance tests were performed over 10 days with 24 h between measurements. Control measurements were also performed with aqueous sodium chloride (NaCl) of concentration 10, 100, 1000 mM and cell medium diluted in purified water to 25% and 50%.

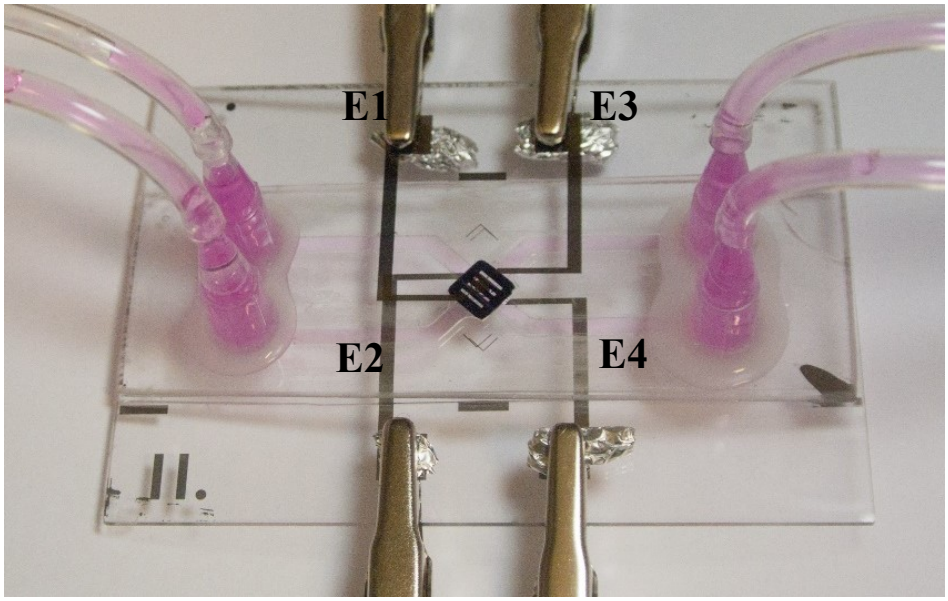

Figure 4.4: Picture taken during impedance measurements. The electrode annotations E1, E2, E3 and E4 was used during the measurements, as well as in the data analysis and presentation.

5. Results

The results obtained during the project consist of: observations from the literature study; two electrode designs (square- and ring electrodes); fabricated electrodes of silver or platinum on glass wafers; and impedance data for electrode testing. The experimental results from the square electrodes and the ring electrodes are presented separately, in different subsections of this chapter, but with a brief comparison of their measurement reproducibility in the end of section 5.4.2.

5.1 Literature study

From the literature study, some important points were brought into consideration. Firstly, a simple method to measure TEER from electrodes placed in the microfluidic channels has been presented by van der Helm et al. [20]. By using four electrodes, two on each side of the membrane, they demonstrate a technique to directly isolate TEER from the system by combining measurements from the four electrodes, without having to perform equivalent circuit modelling. The high resistance from the microfluidic channels, and the associated measurement variations, are directly cancelled out by the model. The model was thus shown to reduce measurement related variations. Their methodology is to measure the impedance between two electrodes for all electrode combinations, a total of six measurements. The impedance values at 10 kHz are then extracted from the impedance spectra and used for the calculation. The measured resistance between two electrodes can be thought of as the sum of the resistances in its path, illustrated in figure 5.1. As there are five unknown resistances and six measurements, Gaussian elimination can then be applied to calculate the individual resistances of the channels, I_1-I_4, and the resistance over the membrane and cellular barrier, I_m. TEER is calculated by formula 4, where A is the cell culture area and $I_{i\text{-}j}$ is the impedance from resistor i to resistor j. TEER is thus directly derived from the resistance I_m. The TEER of the system, measured prior to cell seeding, is subtracted.

$$TEER\ [\Omega\ cm^2] = A\ \times \frac{1}{4}(I_{1\to2} + I_{1\to4} + I_{2\to3} + I_{3\to4} - 2I_{1\to3} - 2I_{2\to4}) \quad (4)$$

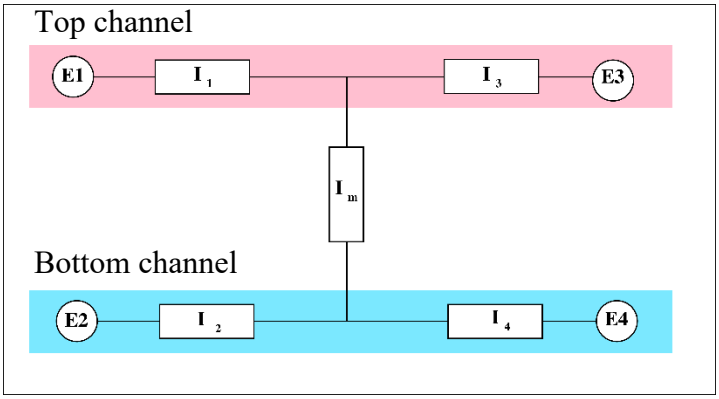

Figure 5.1: Schematic picture of the electrode configuration (adapted from van der Helm et al. [20]*). E1-E4 represent the electrodes, I_1-I_4 the channel resistances and I_m the resistance over the membrane.*

Further, Odjik et al. [5] argue that the current over the cell culture area in a microfluidic organ-on-chip may be unevenly distributed, which can result in a faulty estimation of TEER. The uneven current distribution over the membrane may be due to the geometry of the device or the configuration of the electrodes, and can cause an uneven voltage drop, which gives a faulty estimation of the membrane area. This may lead to an overestimation of TEER. The authors suggest a mathematical model to correct for this effect.

Yeste et al. [31] also discuss this problem as a possible error contributing to the large spread of variation of TEER measurements. From simulation studies on models with different geometries and electrode configurations, they show that the current distribution is dependent on the TEER value and the chamber height of the microfluidic system. The most uniform field is found in systems with a chamber height of 500 µm and larger and for TEER values larger than 10^3 Ωcm^2. The authors propose a formula including a geometric correction factor (GCF) to account for a non-uniform sensitivity field. Further the authors point out placing bipolar electrodes in the inlets and outlets of the system as a limiting factor unless any correction is performed.

Booth et al. [18] suggest that electrodes should be placed directly over the membrane, and cover at least 75% of the membrane area to assure that the resistance measured is representative of the whole membrane. For other electrode placements or electrode sizes, the current density field over the membrane should be considered and accounted for. Van der Helm et al. [20] argues that a uniform distribution across the barrier can be assumed in their model as the barrier resistance is relatively larger than the local channel resistance at the membrane.

TEER has commonly been presented normalised to surface area of the cell culture membrane in the unit Ωcm^2, for easy comparison to other models. A recent article by Henry et al. [19] present TEER in the unit Ω without normalisation to cell culture area, and question the biological significance of Ωcm^2. They argue that the unknown homogeneity of the field and instability in position of hand-manipulated electrodes as well as the influence of indeterminate regions of the cell culture outside the membrane contribute to uncertainties in estimated normalisation area. They also point out that although the cell capacitance is commonly modelled as a capacitor in equivalent circuit models in electrophysiology, constant phase elements (CPE) may be used instead for a better fit of data to the model.

5.2 Electrodes

The two electrode designs that were created are visualised on glass slides in a 3D-drawing below (figure 5.2). The total width of the chip was increased from 25 mm to 51 mm, to allow connection to the electrode pads on both sides.

A complete, functioning fabrication protocol of the electrodes on glass was developed (Appendix A). The fabrication protocol was used for both silver and platinum electrodes. Sputtering of platinum required a considerably higher energy than sputtering of silver. The platinum deposition had to be divided into several parts to not overheat the evaporator. Part of the platinum layer was sputtered, then the system had to cool down before continuing until the desired thickness was reached. It therefore took longer time to fabricate the platinum electrodes. Some artefacts in the photoresist pattern around the tubing holes on the glass was observed, but these did not affect the area of electrode structures and channels.
As the electrodes were fabricated from the same mask they could be replicated with very high precision, with minimal variation in electrode geometry between glass slides. As the chip-layers were manually assembled some variation in alignment occurred in their relative placement. The silver electrodes were very fragile and easily physically damaged and could be wiped off with a paper towel. They were therefore difficult to handle and very often damaged during the bonding process when assembling the device. A brownish layer was sometimes formed on the surface of the silver electrodes during the oxygen plasma bonding to PDMS. Oxidation of silver by the oxygen plasma can result in a reduced conductivity.

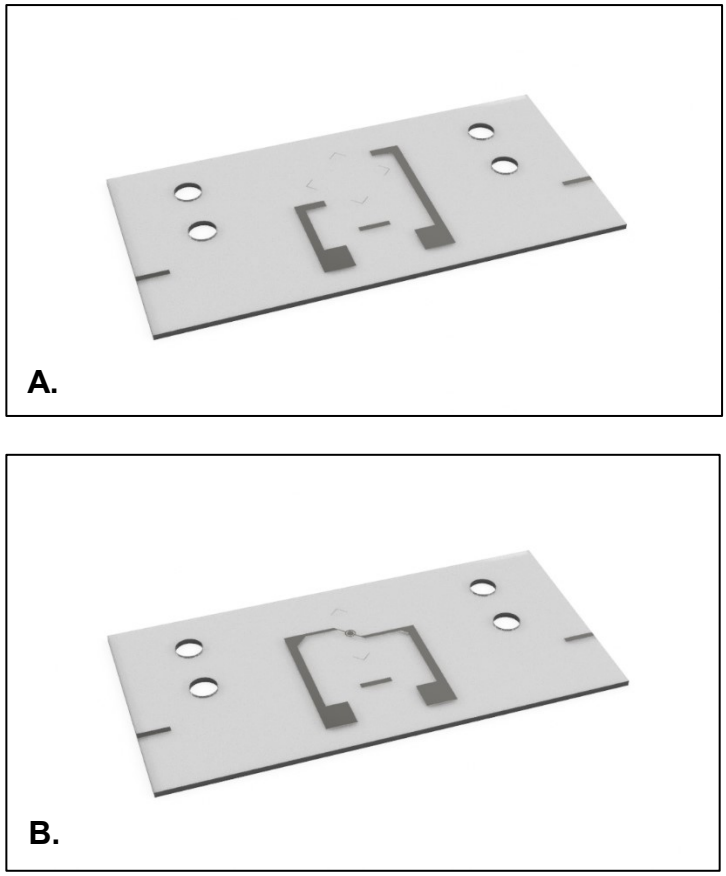

Figure 5.2 Schematic drawing of how the electrodes looks patterned on glass - (A) square electrodes and (B) ring electrodes.

5.3 Impedance measurements: square electrodes

Impedance measurements on chips without cells incorporated were performed to evaluate the performance of the electrodes. The square electrodes were fabricated and tested first, and therefore this design was used for the basic performance tests. Firstly a prototype device, consisting of two electrodes in a single channel was constructed to test if the electrodes could detect a signal. After obtaining satisfactory impedance spectra from the prototype device, impedance measurements were performed on fully assembled chips with and without a

membrane. The experiments aimed to evaluate the choice of material, sensitivity of the electrodes and the reproducibility of the measurements. The sensitivity was tested by measuring the impedance with fluids of different conductivity in the system, and observe if the electrodes could detect a change in conductivity. Measurement reproducibility was tested by reproducing the experiments over a time period up to 10 days, and study the variation between measurements. Efforts were then made to test if combining measurements from all four electrodes can reduce measurement variations of this system.

5.3.1 Characterisation of electrodes in single-channel prototype device

The single channel prototype device that was constructed consisted of one glass layer with thin film electrodes in silver, one layer of PDMS with one channel and a ticker top layer of PDMS (figure 5.3). Very little variation was observed between the measurements (figure 5.4). However, the electrodes were consumed quickly as the silver of the electrodes pads was scraped off when connecting the probes. After four measurements the circuit path was broken and the electrodes could no longer pick up a signal. The number of measurements was therefore limited by damage to the electrode pads. Soldering wires directly to the electrode pads also failed as the thin silver layer was completely oxidized in the process.

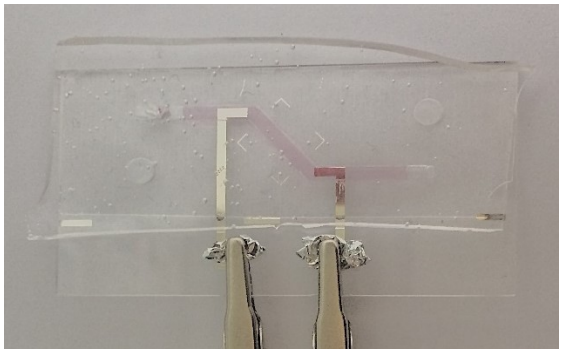

Figure 5.3: Impedance measurement of single-channel prototype device with silver electrodes. Probes from the impedance analyser are clamped to the electrode pads with aluminium foil for better conductivity. The channel was emptied and refilled between all measurements.

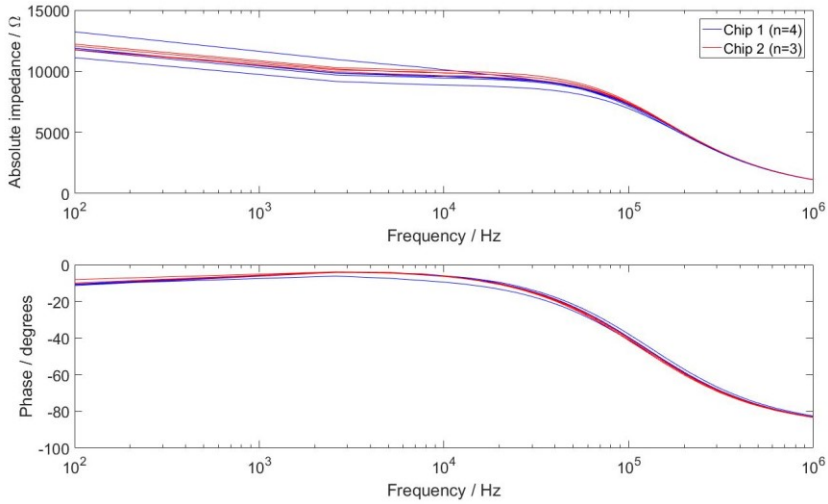

Figure 5.4: Absolute impedance and phase shift spectra derived from the impedance data measured on the prototype device. The highest impedance magnitude, around 1200 Ω, was observed at low frequencies, in the region where the double layer capacitance of the electrodes dominates. The impedance then flattens out in the mid-frequency region, around 10 kHz which is a typically readout frequency for TEER. The phase shift is at a minimum in this region. In the high-frequency range, the impedance magnitude and phase shift both fall rapidly.

5.3.2 Silver electrodes vs. platinum electrodes

Impedance spectra measured with silver electrodes and platinum electrodes are compared in figure 5.5. Measurements were performed on assembled chips without membranes.

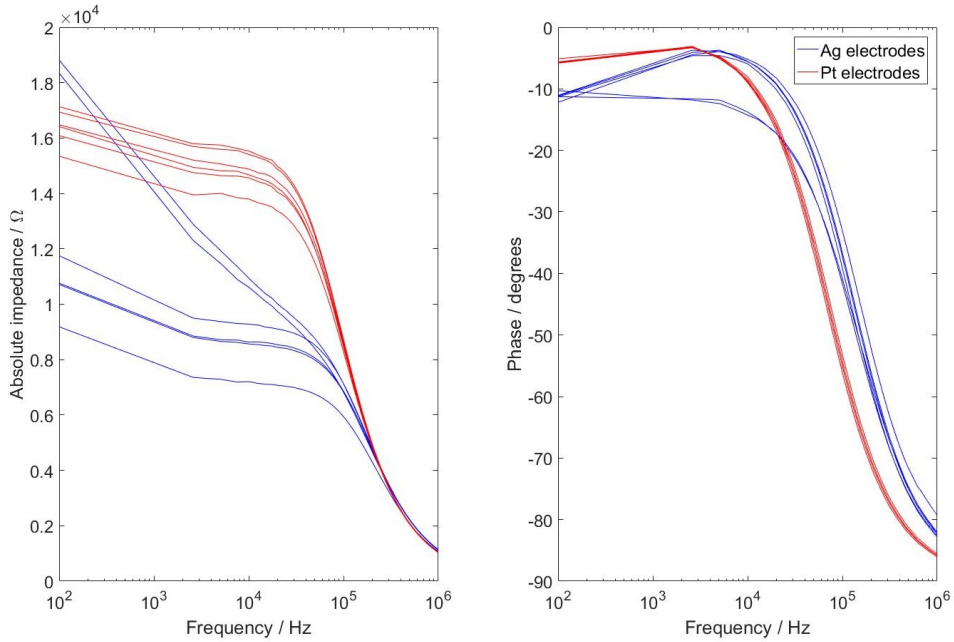

Figure 5.5: Impedance magnitude (left) and phase shift spectra (right) measured on blank chips with platinum electrodes and silver electrodes. Six measurements, one for each combination between the four electrodes, is shown for each chip. Platinum electrodes measured a higher impedance magnitude than the silver electrodes, but with less dispersion in the low- and mid-frequency range. Phase shift spectra of the two metals were comparable.

Silver electrodes and platinum electrodes were both subjected to measurements over 10 days under constant conditions. The silver electrodes failed to reproduce the same spectra already after one measurement (figure 5.6), as the electrode pads were damaged from the probes of the impedance analyser. The platinum electrodes remained physically stable throughout the whole measurement period of 10 days, (figure 5.7).

Blank chip with silver electrodes, day 1

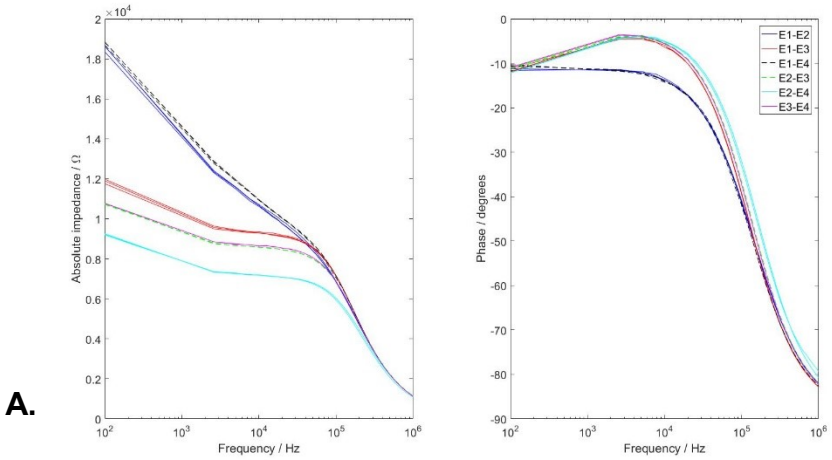

Blank chip with silver electrodes, day 2

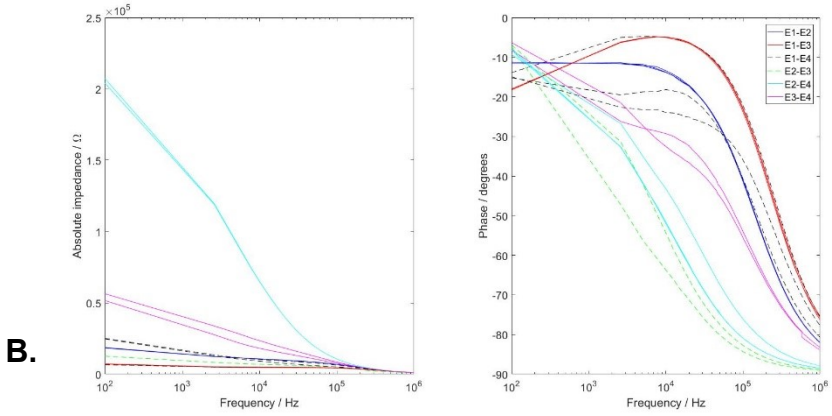

Figure 5.6: Impedance magnitude (left) and phase shift spectra (right) from a blank chip with silver electrodes - (A) Day 1. (B) Day 2.
Dashed lines represent measurements across only one channel and solid lines represent measurements from one channel to another, over the area where the membrane is inserted.

Blank chip with platinum electrodes, day 1

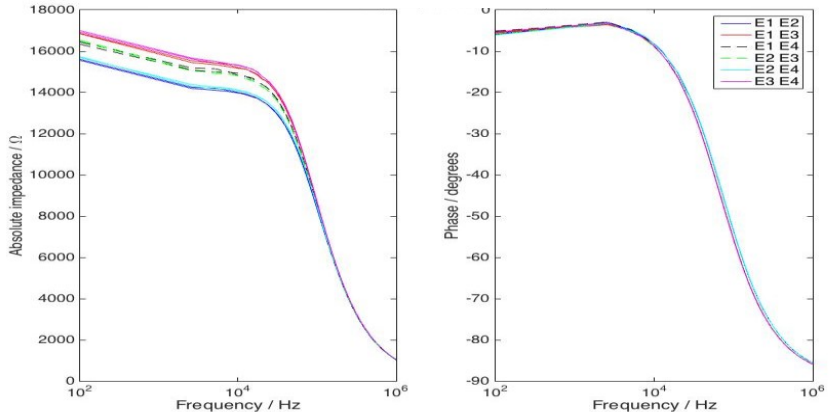

Blank chip with platinum electrodes, day 5

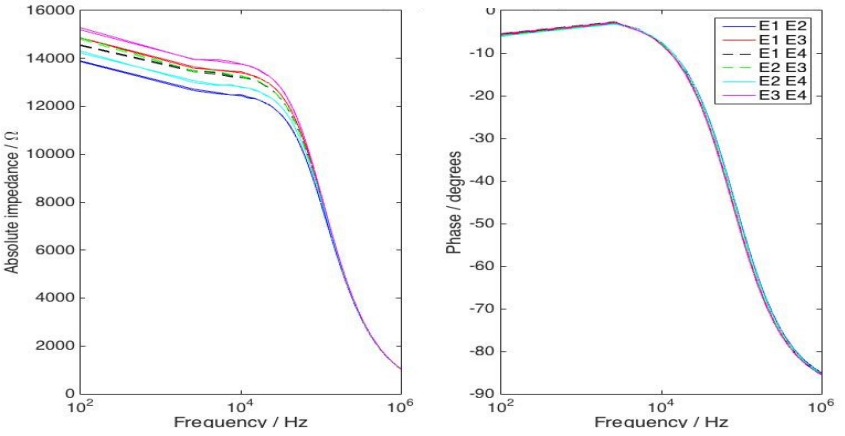

Blank chip with platinum electrodes, day 10

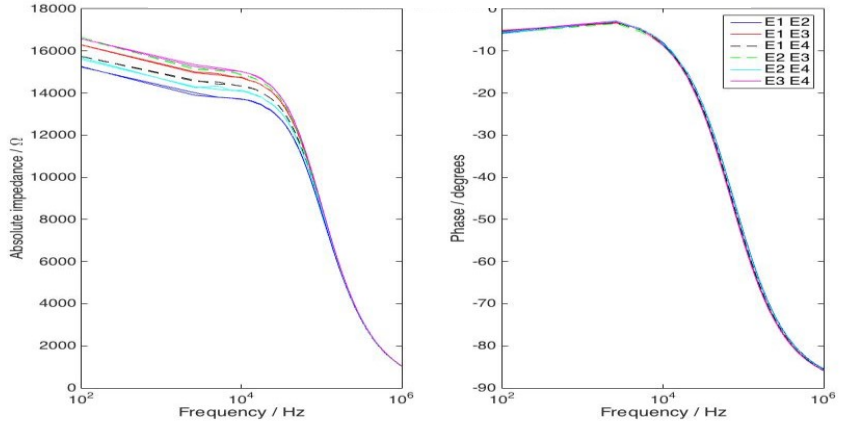

Figure 5.7. Impedance magnitude (left) and phase shift spectra (right) from a blank chip with platinum electrodes - (A) Day 1. (B) Day 5. (C) Day 10.

5.3.3 Characterisation of assembled chips

The impedance spectra from measurements on a fully assembled blank chip and a chip with incorporated membrane measured with platinum electrode are presented in figure 5.8. Some leakage was observed around the membrane of the chip with membrane, which may have influenced the spectra.

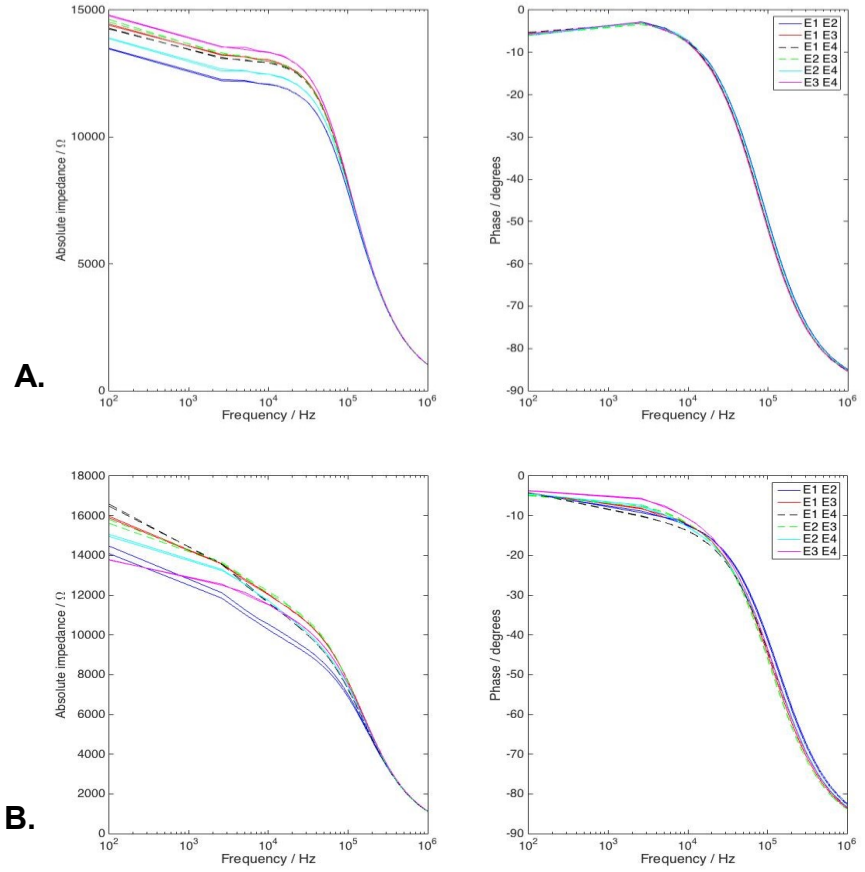

Figure 5.8: Impedance magnitude (left) and phase shift spectra (right) from a (A) blank chip with platinum electrodes and (B) chip with membrane with platinum electrodes. The two chips have comparable impedance magnitudes, although the chip with the membrane seems to have weakened the plateau effect in the mid-frequency range. The chip with membrane also displays more phase shift in the mid-frequency range. Interestingly, these properties were also observed in the measurements between electrodes in the same channel that do not measure across the membrane.

5.3.4 Sensitivity test

Tests performed with NaCl and diluted medium show that the electrodes are sensitive to a change in electrolyte conductivity (figure 5.9). The medium was estimated to have a conductivity close to 100 mM NaCl, which agrees with the results obtained.

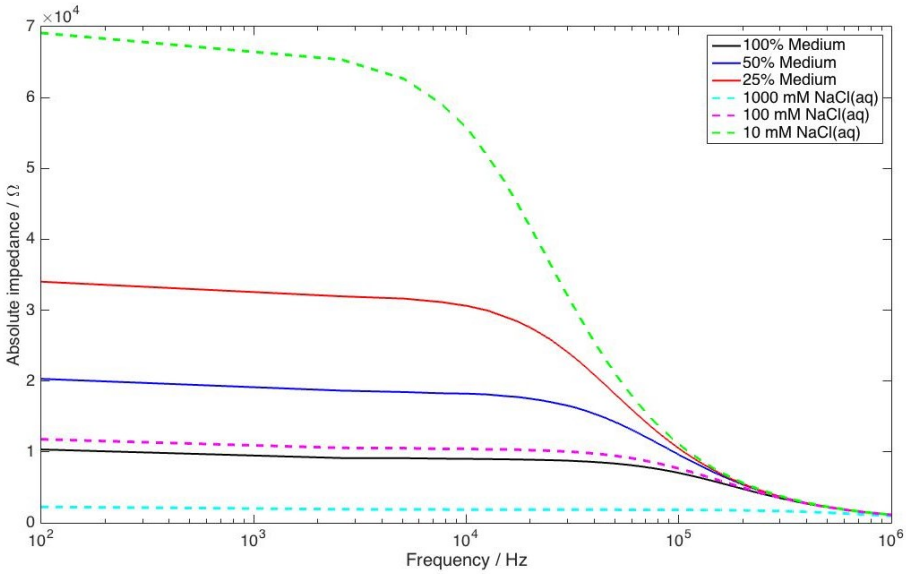

Figure 5.9: Impedance magnitude measured on a blank chip with platinum electrodes, filled with different electrolyte of varying conductivity. A low conductivity results in higher impedance.

5.3.5 Reproducibility test

Measurements on two blank chips were performed daily under constant conditions over 10 days to observe the reproducibility of the measurements. The impedance value at 10 kHz has been extracted from all measurements and is presented in figure 5.10, to illustrate the measurement variations. The figure also shows the same measurements performed on a chip with membrane, Chip C, over 5 days.
Chip A had some small parts of incomplete bonding between the top glass and PDMS-layer. Chip B was assembled when the bonding protocol had been optimised. Large measurements variations between days were observed for all chips, especially for Chip A and Chip C which had not bonded completely.

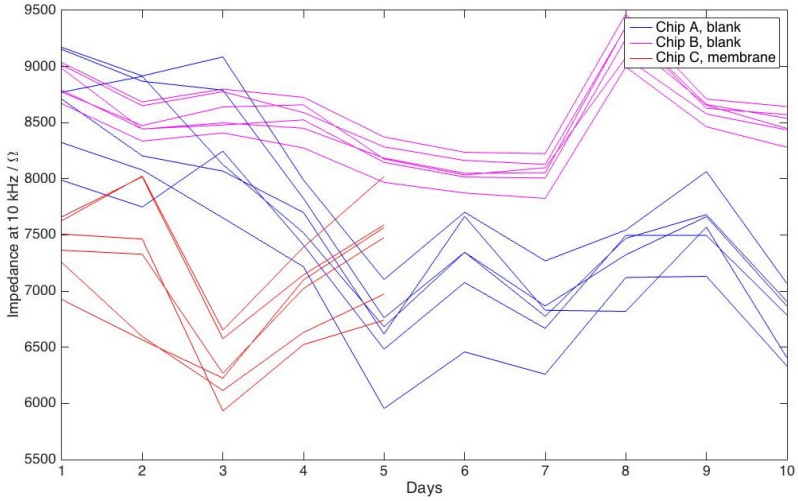

Figure 5.10: Impedance at 10 kHz measured over 10 days for two blank chips, Chip A and Chip B, and one chip with membrane, Chip C. The graph shows the measured impedance for all electrode combinations.

A protocol of combining measurements from the four electrodes, based on the article by van der Helm et al. [20], was created attempting to isolate the impedance over the cell membrane, I_m, from which TEER can be directly calculated. Figure 5.11 presents the derived I_m, isolated from the impedance of the channels. Although there is still some variation, I_m has much less variation than the measured impedances in figure 5.10 for all 3 chips.

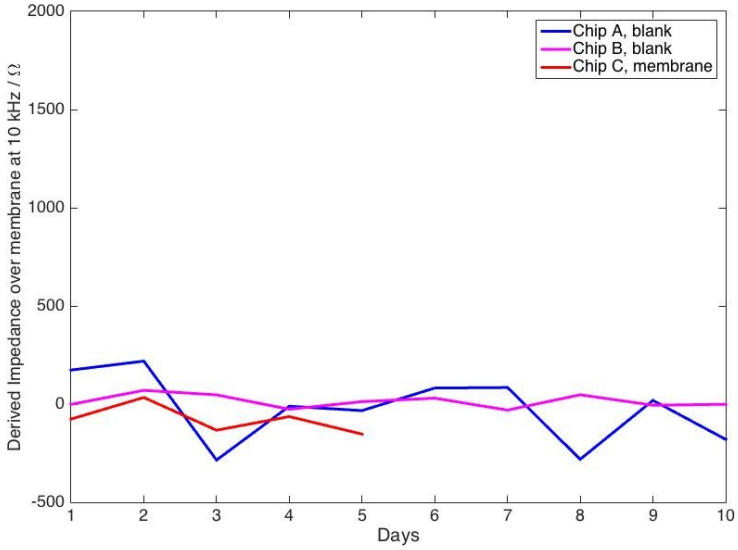

Figure 5.11: Impedance I_m , derived from combining the measurements in Figure 5.10.

5.4 Impedance measurements: ring electrodes

After characterising the square electrodes, the ring electrodes were fabricated in platinum and tested in the same way. As they are placed much closed to each other than the square electrodes, the impedance measured between the ring electrodes was hypothesised to be lower than the square electrodes. Ring electrodes were only fabricated in platinum.

5.4.1 Characterisation of an assembled chips

Impedance spectra measured from the ring electrodes are presented in figure 5.12 A. As expected, the impedance measured from the ring electrodes is lower than the impedance of the same system with the square electrodes.
Impedance spectra measured on a system with incorporated membrane is presented in figure 5.12 B. When comparing the spectra from the blank chip and the chip with membrane, there was no apparent difference as a result of the membrane.

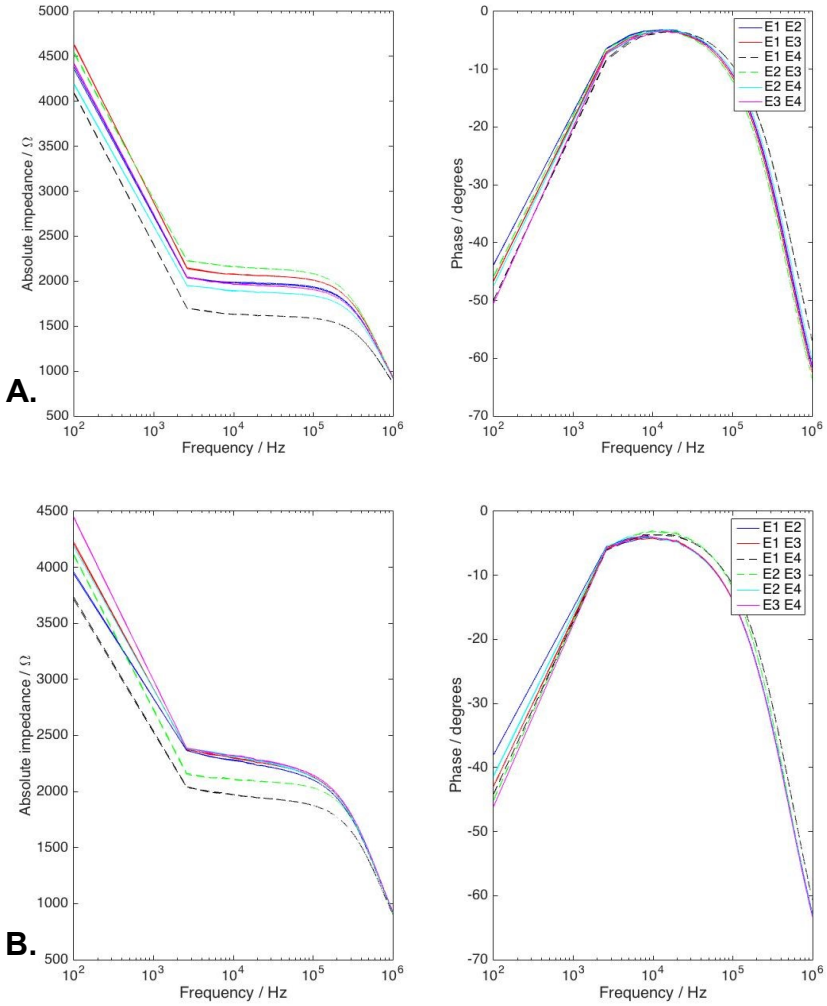

Figure 5.12: Impedance magnitude (left) and phase shift spectra (right) from a (A) blank chip with platinum ring electrodes and (B) chip with membrane with platinum ring electrodes. In the mid-frequency range, a plateau at an impedance of approximately 2 kΩ is formed. The smallest phase shift is observed around 10 kHz.

5.4.2 Sensitivity test

The ring electrodes are also sensitive to a change in electrolyte conductivity (figure 5.13). The medium had an impedance close 100 mM NaCl, as expected.

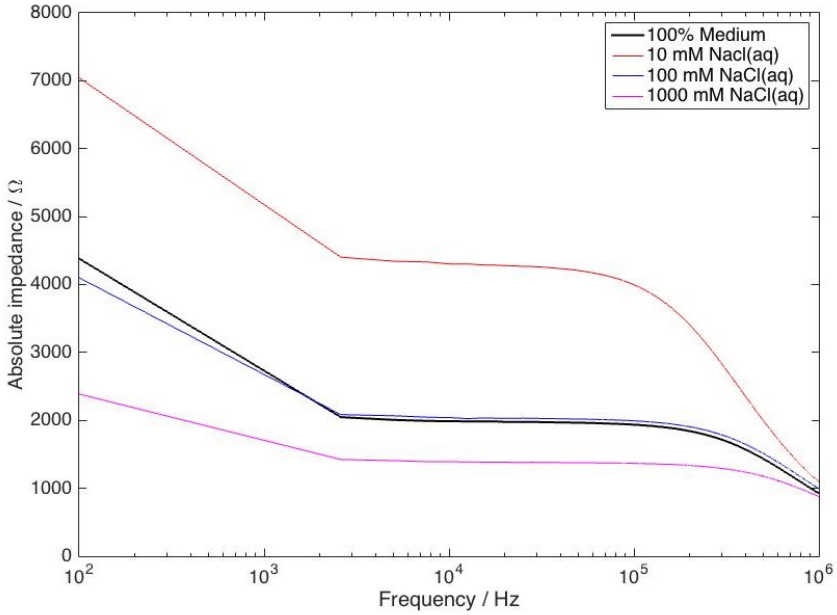

Figure 5.13: Impedance magnitude measured on a blank chip with platinum electrodes, filled with different electrolytes of varying conductivity. A low conductivity results in higher impedance.

5.4.3 Reproducibility test

The blank chip tested over 10 days, and found to produce stable spectra throughout the measurement period. A chip with membrane was studied over 3 days. Like for the square electrodes, the impedance at 10 kHz was extracted and plotted to study measurement variations (figure 5.14). Some variation between measurements was observed, but less than for the square electrodes.
Also, the same procedure of combining measurements to derive I_m was performed for the ring electrodes (figure 5.15). I_m derived from combining measurements was of similar magnitude as for the square electrodes. A reduction in variation was also observed, however the difference was less significant than for the square electrodes as the measurement from the ring electrodes showed much less variation from the start.

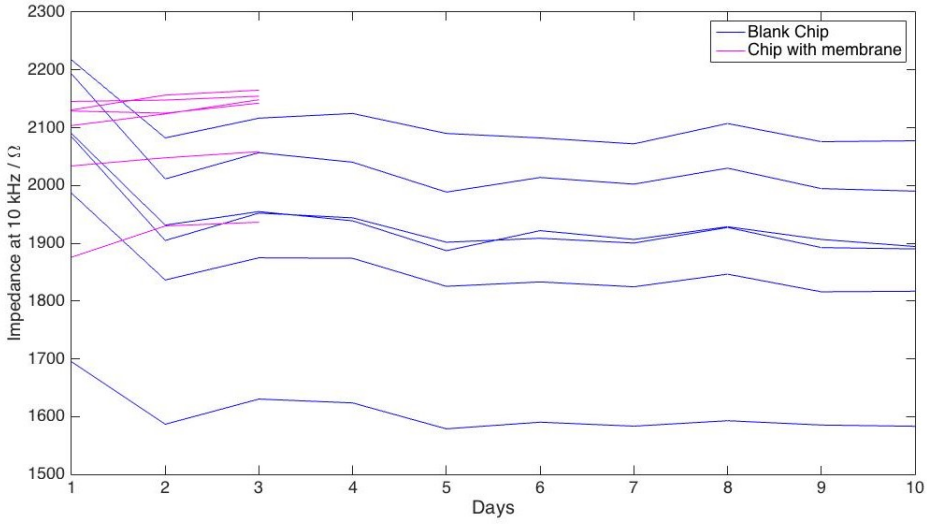

Figure 5.14: Impedance at 10 kHz measured over 10 days for a blank chip, and a chip with membrane. The graph shows the measured impedance for all electrode combinations.

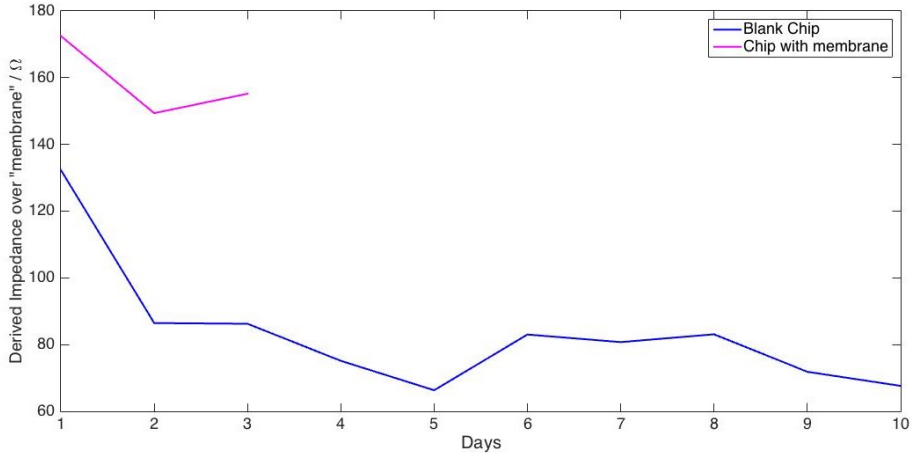

Figure 5.15: I_m, derived from combining the measurements in Figure 5.14.

To further illustrate the difference in variation, standard error of mean (SEM) values for were calculated for all measurements and their derived I_m (figure 5.16). SEM values were normalised to the membrane area for easy comparison to reported uncertainly values of TEER in literature. SEM is proportional to the mean value. Therefore, as the mean values of measured impedance from the square electrodes are much larger than from the ring electrodes, in the range of 5-10 times larger, there is no statistical relevance to comparing their SEM values.
However, I_m is expected to be of the same magnitude for all chips. SEM values of the calculated I_m are lower for the ring electrodes, indicating less variation compared to the square electrodes. Chip A and chip C which were observed to leak, had SEM values between 1-2 Ωcm^2, and the 3 remaining chips had SEM values less than 0.5 Ωcm^2. It can also be seen in the figure that SEM values of I_m are of similar magnitude as all measurements performed with the ring electrodes.

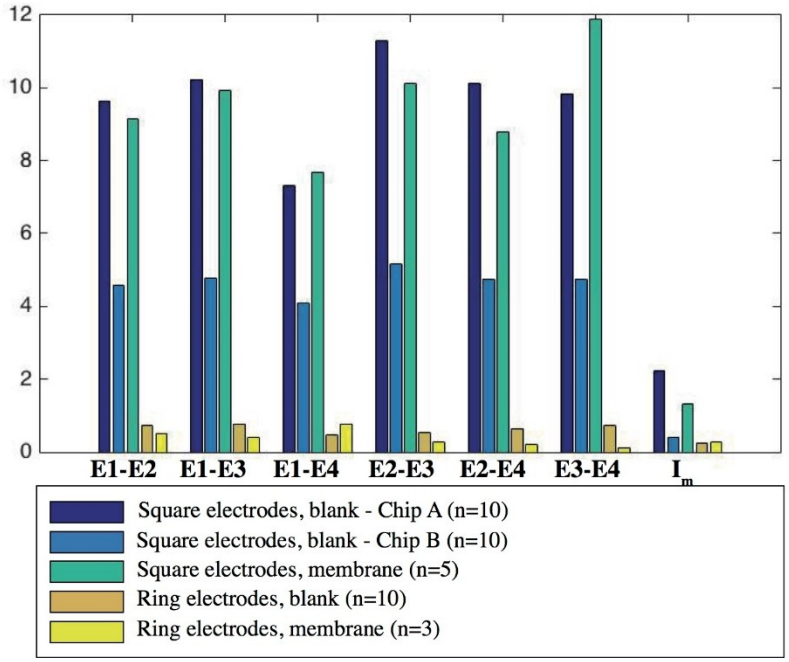

Figure 5.16: Calculated SEM for all measurements and their derived I_m,

6. Discussion

The main factor considered when selecting a material was to ensure that the electrodes do not risk harming the cells. Further, the material must endure several measurements without being damaged. As no measurements with cells have been performed in this study, the biocompatibility of electrodes cannot be compared. As previously stated, platinum and Ag/AgCl electrodes are not expected to harm the cells. Also, as the flow rate in the device is high, there is a small risk of particles from the electrode lingering on the cells. Silver and platinum were also chosen as they both have been studied before, making it possible to benchmark to other studies. Silver electrodes can be chlorinated to form AgCl by dipping the electrodes into diluted ferric chloride solution, or by flushing diluted ferric chloride solution through the channels. This was not performed as the silver electrodes failed the first measurements and was thereafter discarded. Chlorinating the silver electrodes has been shown to improve the chemical stability [32], but is unlikely to improve the physical stability, which in this case was the main issue. From a fabrication perspective, Ag/AgCl electrodes have the disadvantage of chlorination procedures and poor physical stability, whereas platinum electrodes require more efforts to fabricate. Overall, platinum was concluded to be the more suitable material. Silver was discarded because of the poor physical stability of the electrodes. Based on observations, gold might be a good alternative due to a combination of inertness and fabrication advantages. However, there are few related studies on gold electrodes, limiting the potential of benchmarking results.

From the literature study, limitations to placing electrodes in the channels were noted. In this project, a problem observed with the electrodes over the membrane was that they block the field of view. Cells can therefore not be inspected under a microscope, and it was difficult to see if air bubbles were trapped around the membrane. In that sense, electrodes placed out in the channels, away from the membrane are preferred. Another advantage of placing the electrodes out in the channels was that the electrodes could be made larger. This is of less significance, as the ring electrodes did not appear to have considerably higher noise level than the larger square electrodes. The main drawback of the square electrodes was that the measured system was impeded by more fluid, resulting in a higher baseline impedance, prone to more variation. The ring electrodes were also more difficult to align with precision due to their small size, which could contribute to variances between chips. From a fabrication perspective, there was no difference between the two designs. The same fabrication protocol could be used, and there were no problems making the small structures of the ring electrodes.

Both electrode designs could detect a change in medium conductivity. The conductivity of the cell culture medium is unknown, but from the results it is shown to have a conductivity close to 100 mM $NaCl_{(aq)}$.

As 10 kHz often is used as a readout frequency for TEER, it was selected as the frequency for analysing variations. All chips also showed the lowest phase shift around 10 kHz, indicating that the system was least capacitive in this region. After having characterised the spectra obtained from the square electrodes and the ring electrodes and their sensitivity, the experiments focused on reproducibility. A stable baseline for the chip without cells is important for the quality of the TEER measurements, as variations in the baseline can give a faulty estimation of TEER. It was evident that measurement variations occurred even though efforts were made to minimise errors both during bonding and measurements. Chips and electrodes were designed to be perfectly symmetrical, and the theoretical impedance between the electrodes is thus equal. Yet there were differences within a chip, as well as between chips of identical designs. As the chips are manually assembled, some variation in electrode placement between chips is unavoidable. However, this variation only affects the system baseline as electrodes remain fixed after the chip is assembled and does not cause any variation between measurements. Furthermore, some variation is thought to originate from small air bubbles in the system. Measuring at a flow and using a bubble trap system will decrease the risk of bubble formation.

Ring electrodes fabricated in platinum could measure impedance at the highest precision. Measurement variation from the square electrodes was observed to be around 10 times larger than for the ring electrodes. It can thus be assumed that the square electrodes are not sensitive enough to measure TEER directly from one measurement. However, measurement variation in the channels was effectively reduced by combining measurements from the four electrodes to isolate the impedance over the membrane. To our knowledge, no similar study has been performed on fully integrated thin film electrodes. It was also noted that combining measurements did not significantly reduce the SEM values for the ring electrodes. It can thus be argued that the ring electrodes can measure TEER with the same precision directly with only one measurement. It should also be noted that there are additional sources of variation when measurements are performed on cells, such as biological variation and confluency of the cell layer.

Several limitations to the study were identified. Firstly, only one chip of each type was used for the analysis. For a more comprehensive assessment more chips would have to be studied, especially as there is assumed to be some chip to chip variation and as some chips were leaking. Also, all measurements were performed under static conditions. The electrode properties under flow conditions have thus not been evaluated.

Further, due to a drawing mistake of the ring electrodes, the metal structures connecting the sensing area to the electrode pads in the ring design can be seen to cross the microfluidic channels for two out of four electrodes (see figure 4.1 B). This did not appear to have an effect on the results in this study, presumably because the distance between the sensing electrode structures is several magnitudes lower than the distance out to the exposed metal in the channel. However, this was corrected for in the design, and if more electrodes were to be fabricated the mask of the corrected design presented in figure 6.1 should be used.

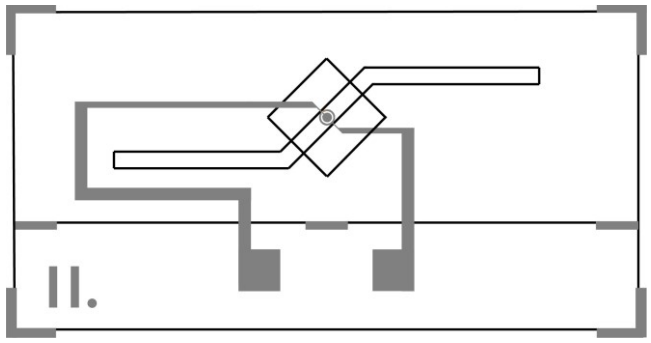

Figure 6.1: Drawing of the corrected ring electrode design, adapted from the CAD-drawings.

6.1 Possibilities to derive TEER

The electrodes developed aim to be used to measure TEER in the microfluidic device. The study demonstrated that both electrode designs can measure the impedance of the system, but no measurements with living cells in the chips were performed. As no actual TEER measurements on cells have been performed, the suggestions for TEER measurements discussed in this chapter are merely speculations based on the impedance measurements of the system. To study the quality of the TEER measurements, measurements must be performed with cells cultured in the systems. It is likely that additional factors influencing the choice of measurement technique or electrode design will appear when cells are added.

Based on previously published studies, measuring TEER with electrodes in the microfluidic channels without any correction has been advised against due to the risk of inhomogeneity in the current field over the membrane. Therefore, computer simulations to study the current field should be performed on the square

electrodes before these are used for TEER measurements. This is also recommended to validate of the ring electrodes. If needed, mathematical correction to compensate for uneven current fields can be applied retrospectively.

There are two advantages of integrating four electrodes for TEER measurements rather than two. Firstly, 4-point impedance measurements can be performed to separate the current path from the measured voltage. This simplifies the subsequent interpretation as the impedance of the measuring system is excluded. An equivalent circuit model of only the cellular parameters and the resistance of the medium can thus be used. Also, only one measurement needs to be performed. This method is assumed to be suitable for the ring electrodes that are placed close to the membrane, but less suitable for the square electrodes as they are placed further away and therefore prone to more variation from the medium in the channels.

Secondly, by performing 2-point measurements for all combinations of the four electrodes, the impedance over the membrane from which TEER is calculated can be directly isolated from the total impedance. The main advantages of this method are that electrodes can be placed further from the membrane and that simple resistance measurements can be performed instead of impedance measurements. Thus, the bulky impedance analyser, that may not be available in cell laboratories, would not be needed. However, 6 measurements need to be performed instead of one. Another drawback of this simple method to derive TEER is that the derived resistance represents all impeding cellular components rather than only the TEER value. With only resistance measurements the capacitance of the cell membrane cannot be extracted. To obtain a value for only TEER resulting from tight junction formation, the same measurements must be performed directly after cell seeding in the system, before tight junctions are formed, and then subtracted from the measurements after tight junctions have formed. If impedance measurements are performed, an equivalent circuit with parameters representing the cell layer could speculatively be applied to extract the individual parameters from the total derived impedance. There are however no reported studies on this.

One risk of combining measurements would be that the impedance of cells is also cancelled out from the formula. To ensure that this is not the case, measurements on cells must be performed to compare the spectra from chips before and after cell seeding. There should also be a difference between impedance measured from electrodes placed in the same channel (that do not measure over the membrane and cells) and impedance measured over the cell membrane.

The advantages of the ring electrodes that were presented were rather a consequence of their placement close to the cell culture area and not their shape. It could be further investigated whether the ring shape has any advantages over making a simpler square design. To avoid the problem of electrodes blocking the

field of view and limiting visual inspection electrodes could be made thinner, approximately 40 nm thick, which would make the electrodes invisible. However, it is assumed to be problematic making platinum electrodes this thin with a uniform thickness. Gold is thought to be a more suitable material for making very thin electrodes.

6.2 Ethical reflection

The use of animal experiments in biomedical research is motivated by obtaining new information about diseases and the human physiology that could potentially improve therapeutic strategies and treatments. In pharmaceutical development, animal experiments are often a necessary step in the process of taking a new drug to the clinical phase.

To minimise the use of laboratory animals, the principle of the three R's: Refine, Reduce and Replace, can be applied [33]. The three R's aim to replace animal experiments with alternative methods. The framework has been implemented in international legislation controlling the use of laboratory animals for scientific applications.

In vitro models provide an ethical alternative to animal models. They aim to isolate specific structures and functions of the human body, rather than representing the complexity of a full body, or a full brain. Many types of tests can only be made on animals in order to validate the complex interplay of organs and metabolism. *In vitro* models can therefore not fully replace animal testing, but reduce them towards a minimal involvement of animals for scientific research and drug discovery.

In vitro models of the blood-brain barrier show great potential for application in the early stages of drug development. Many potential drugs for treatment of disorders in the CNS fail because they cannot penetrate the blood-brain barrier. Efforts and resources can be saved if BBB permeability can be tested earlier in the process. This is a main driving force in the development of better *in-vitro* models of the BBB, and can eventually lead to more ethical and sustainable development of pharmaceuticals, food and cosmetics.

7. Conclusions and future aspects

In this Master's thesis project, microelectrodes for electrical measurements were integrated in a microfluidic BBB-model. In attempt to find an optimal electrode design and configuration for TEER measurements, two electrode designs were developed and evaluated with respect to their measurement reproducibility and sensitivity.

It can be concluded from this study that electrodes placed in the microfluidic channels, at a distance from the cell culture area, showed much larger measurement variations compared to electrodes placed directly over the cell culture area. However, a technique of combining measurements from four electrodes was applied to effectively reduce measurement related variations from electrodes placed in the channels. Further, both electrode designs had sufficient sensitivity to detect and change in medium conductivity. Platinum was concluded to be a better electrode material for TEER measurement than silver, due to poor physical stability of the silver electrodes.

Based on the results from this study in combination with a review of previously published studies, methods to derive TEER are discussed. Although the electrodes that were developed are believed to provide sufficient sensitivity and robustness to be used for TEER measurements, further improvements can be made to the geometry and material of the electrodes as well as to the practicality around the measurement procedure. To evaluate the performance of the electrodes for TEER measurements, further testing with cells in the device is be needed. If more time was available, the next step would be to culture cells in the device and test if barrier formation could be monitored with measurements from the integrated electrodes. The equivalent electrical circuit that was suggested could be fitted to the data to derive the TEER of the cell culture. Further evaluation on whether the method of combining measurements from four electrodes is an accurate technique to derive TEER in this microfluidic system must also be performed when cells are cultured in the system. Numerical computer simulations should be performed to study the electric current field in the system.

TEER measurements in microfluidic models remain a challenge. However, recent advances with fully integrated electrodes, such as demonstrated in this project, enable more accurate TEER measurements *in situ*. Improved TEER measurements offers a reliable quantitative validation parameter that may potentially accelerate the development of BBB-on-chip models.

8. Appendices

Appendix A – Microfabrication protocols

A1. Mask fabrication

1. Create the mask in a mask writer (Heidenberg Instrument DWL66).
2. Place the mask in developer solution (Microposit 351, dil 1:4) for 1 minute.
3. Wash the mask in Milli-Q water and blow-dry with nitrogen gas until dry.
4. Etch the mask in chromium etchant solution for 1 minute.
5. Wash the mask in Milli-Q water and blow-dry with nitrogen gas until dry.
6. Observe in microscope.

A2. Spin coat negative resist on glass wafer

1. Wipe off the glass slide to make sure there is no dust on the surfaces.
2. Position the glass wafer in a 3D-printed custom-made holder on the chuck in the spin coater.
3. Apply the settings 2000 rpm / 30 seconds to the spin coater, for a resulting layer thickness of 4 μm.
4. Place 2 ml of negative photoresist (AZ nLOF 2020 neg. dil 1:0,40 2.0 μm, AZ Electronic Materials GmbH) on the glass using a pipette.
5. Start the spin coater.
6. Prebake the glass slide with resist on a hotplate for 1 minute at a temperature of 100 °C.

A3. UV lithography

1. Place the glass wafer on the sample plate of the mask aligner.
2. Place the photomask directly on top of the wafer with the chromium side facing down towards the wafer.
3. Press the button “Load” to position the wafer for UV exposure.
4. Expose to UV-light for 9 seconds.
5. Carefully remove the wafer and the photomask.
6. Postbake the glass wafer on a hotplate for 1 minute at a temperature of 110 °C.

A4. Development of photoresist

1. Submerge the wafer in a beaker containing developer solution (AZ 326) for 25 seconds while carefully twirling the beaker. Pick up the wafer with a tweezer.
2. Wash the wafer by placing it in a beaker with Milli-Q water for 20 seconds while twirling.
3. Blow-dry the wafer with nitrogen gas until dry.
4. Observe the structures in microscope.

A5. Metal deposition and Lift-off

1. Clean the wafer by plasma cleaning with oxygen gas for 3 minutes in a plasma oven (Diener Femto).
2. Place the clean wafer in a thin film deposition system (Auto 306 Vacuum Coating System, BOC Edwards) and operate according to the manual of the system.
3. Deposit a layer of 30-40 nm of Ti over the wafer by vacuum evaporation.
4. Subsequently deposit a layer of 200 nm of silver, or 150 nm of platinum by electron beam physical vapour deposition.
5. Carefully remove the wafer and let it cool down.
6. “Lift-off” using the developer dimethyl sulfoxide, dehydrated (VWR Chemicals) preheated to 80 degrees over water bath. Leave the wafer in the developer solution under ultrasonication until the polymer has dissolved (approximately 30 seconds).
7. Rinse in water and blow dry with nitrogen gas.
8. Wash glass wafer with electrodes in a dishwasher. The fabrication process is now complete.

Appendix B – Impedance Measurement Protocol

1. Place the chip in a beaker filled with water. Place the beaker containing the chip in a vacuum pump at 25 inHg for 1 hour to drive off air trapped in the membrane.
2. Prepare the cell culture medium. Carefully swirl the medium in a plastic test tube. If much bubbles are present in the medium, degas the medium in a vacuum pump.
3. For static measurements: Fill channels slowly with the modified cell culture medium (DMEM) using a syringe. Filling of channels can be done from one or several inlets simultaneously.
4. No air bubbles should be present in the system. Let the medium reach room temperature before starting the measurements.
5. Make sure the impedance analyser is connected to the lab computer via a DAQ-cable for data transfer from the impedance analyser.
6. Connect the cables from the impedance analyser (HP4194A, Hewlett-Packard, Palo Alto, USA) to the electrode pads with clamps. Use a small piece of aluminium foil between the clamp and the electrodes for better connection.
7. Use a custom-made matlab function (F_Sweep) to perform impedance measurements over a frequency sweep, and to derive and collect impedance data. Specify start frequency, end frequency and number of data points as function inputs. The function presents the impedance magnitude and phase shift as a function of frequency.
8. Measure impedance as in point 7. between all electrodes (Ei-Ej), according to the scheme below (Table B.1). A total of 6 measurements should be performed.

Measurement number	Electrodes
1	E1 – E2
2	E1 – E3
3	E1 – E4
4	E2 – E3
5	E2 – E4
6	E3 – E4

Table B.1 Impedance measurement scheme

10. References

[1] Capulli, M., O. K. Olstad, P. Onnerfjord, V. Tillgren, M. Muraca, K. M. Gautvik, D. Heinegård, N. Rucci & A. Teti (2014) The C-terminal domain of chondroadherin: a new regulator of osteoclast motility counteracting bone loss. *J Bone Miner Res,* 29**,** 1833-46.

[2] Bhatia, S. N. & D. E. Ingber (2014) Microfluidic organs-on-chips. *Nat Biotechnol,* 32**,** 760-72.

[3] Meer, A. D. v. d. & A. v. d. Berg (2012) Organs-on-chips: breaking the in vitro impasse. *Integrative Biology,* 4**,** 461-470.

[4] Srinivasan, B., A. R. Kolli, M. B. Esch, H. E. Abaci, M. L. Shuler & J. J. Hickman (2015) TEER measurement techniques for in vitro barrier model systems. *J Lab Autom,* 20**,** 107-26.

[5] Odijk, M., A. D. van der Meer, D. Levner, H. J. Kim, M. W. van der Helm, L. I. Segerink, J. P. Frimat, G. A. Hamilton, D. E. Ingber & A. van den Berg (2015) Measuring direct current trans-epithelial electrical resistance in organ-on-a-chip microsystems. *Lab Chip,* 15**,** 745-52.

[6] Kamiya, A., R. Bukhari & T. Togawa (1984) Adaptive regulation of wall shear stress optimizing vascular tree function. *Bull Math Biol,* 46**,** 127-37.

[7] Abbott, N. J., A. A. Patabendige, D. E. Dolman, S. R. Yusof & D. J. Begley (2010) Structure and function of the blood-brain barrier. *Neurobiol Dis,* 37**,** 13-25.

[8] Pardridge, W. M. (1999) Blood-brain barrier biology and methodology. *J Neurovirol,* 5**,** 556-69.

[9] Wong, A. D., M. Ye, A. F. Levy, J. D. Rothstein, D. E. Bergles & P. C. Searson (2013) The blood-brain barrier: an engineering perspective. *Front Neuroeng,* 6**,** 7.

[10] Wolff, A., M. Antfolk, B. Brodin & M. Tenje (2015) In Vitro Blood-Brain Barrier Models-An Overview of Established Models and New Microfluidic Approaches. *J Pharm Sci,* 104**,** 2727-46.

[11] Hackam, D. G. (2007) Translating animal research into clinical benefit. *BMJ,* 334**,** 163-4.

[12] van der Helm, M. W., A. D. van der Meer, J. C. Eijkel, A. van den Berg & L. I. Segerink (2016b) Microfluidic organ-on-chip technology for blood-brain barrier research. *Tissue Barriers,* 4**,** e1142493.

[13] Thuenauer, R., E. Rodriguez-Boulan & W. Römer (2014) Microfluidic approaches for epithelial cell layer culture and characterisation. *Analyst,* 139**,** 3206-18.

[14] Crone, C. & S. P. Olesen (1982) Electrical resistance of brain microvascular endothelium. *Brain Res,* 241**,** 49-55.

[15] Butt, A. M. & H. C. Jones (1992) Effect of histamine and antagonists on electrical resistance across the blood-brain barrier in rat brain-surface microvessels. *Brain Res,* 569**,** 100-5.

[16] Santaguida, S., D. Janigro, M. Hossain, E. Oby, E. Rapp & L. Cucullo (2006) Side by side comparison between dynamic versus static models of blood-brain barrier in vitro: a permeability study. *Brain Res,* 1109**,** 1-13.

[17] Wang, Y. I., H. E. Abaci & M. L. Shuler (2017) Microfluidic blood-brain barrier model provides in vivo-like barrier properties for drug permeability screening. *Biotechnol Bioeng,* 114**,** 184-194.

[18] Booth, R. & H. Kim (2014) Permeability analysis of neuroactive drugs through a dynamic microfluidic in vitro blood-brain barrier model. *Ann Biomed Eng,* 42**,** 2379-91.

[19] Henry, O. Y. F., R. Villenave, M. J. Cronce, W. D. Leineweber, M. A. Benz & D. E. Ingber (2017) Organs-on-chips with integrated electrodes for trans-epithelial electrical resistance (TEER) measurements of human epithelial barrier function. *Lab Chip,* 17**,** 2264-2271.

[20] van der Helm, M. W., M. Odijk, J. P. Frimat, A. D. van der Meer, J. C. T. Eijkel, A. van den Berg & L. I. Segerink (2016a) Direct quantification of transendothelial electrical resistance in organs-on-chips. *Biosens Bioelectron,* 85**,** 924-929.

[21] Griep, L. M., F. Wolbers, B. de Wagenaar, P. M. ter Braak, B. B. Weksler, I. A. Romero, P. O. Couraud, I. Vermes, A. D. van der Meer & A. van den Berg (2013) BBB on chip: microfluidic platform to mechanically and biochemically modulate blood-brain barrier function. *Biomed Microdevices,* 15**,** 145-50.

[22] Douville, N. J., Y. C. Tung, R. Li, J. D. Wang, M. E. El-Sayed & S. Takayama (2010) Fabrication of two-layered channel system with embedded electrodes to measure resistance across epithelial and endothelial barriers. *Anal Chem,* 82**,** 2505-11.

[23] Reichel, A., D. J. Begley & N. J. Abbott (2003) An overview of in vitro techniques for blood-brain barrier studies. *Methods Mol Med,* 89**,** 307-24.

[24] Barsoukov, E. & J. R. Macdonald. 2005. *Impedance spectroscopy : theory, experiment, and applications*. Hoboken, N.J.: Wiley-Interscience.

[25] Benson, K., S. Cramer & H. J. Galla (2013) Impedance-based cell monitoring: barrier properties and beyond. *Fluids Barriers CNS,* 10**,** 5.

[26] Wegener, J. & J. Seebach (2014) Experimental tools to monitor the dynamics of endothelial barrier function: a survey of in vitro approaches. *Cell Tissue Res,* 355**,** 485-514.

[27] Kottra, G. & E. Frömter (1984) Rapid determination of intraepithelial resistance barriers by alternating current spectroscopy. II. Test of model circuits and quantification of results. *Pflugers Arch,* 402**,** 421-32.

[28] Temiz, Y., A. Ferretti, Y. Leblebici & C. Guiducci (2012) A comparative study on fabrication techniques for on-chip microelectrodes. *Lab Chip,* 12**,** 4920-8.

[29] Sarró, E., M. Lecina, A. Fontova, C. Solà, F. Gòdia, J. J. Cairó & R. Bragós (2012) Electrical impedance spectroscopy measurements using a four-electrode configuration improve on-line monitoring of cell concentration in adherent animal cell cultures. *Biosens Bioelectron,* 31**,** 257-63.

[30] Folch, A. 2013. *Introduction to bioMEMS*. Boca Raton: CRC Press.

[31] Yeste, J., X. Illa, C. Gutiérrez, M. Solé, A. Guimerà, R. Villa (2016) Geometric correction factor for transepithelial electrical resistance measurements in transwell and microfluidic cell cultures. *Journal of Physics D: Applied Physics,* 49**,** 375401.

[32] Polk, B. J., A. Stelzenmuller, G. Mijares, W. MacCrehan & M. Gaitan (2006) Ag/AgCl microelectrodes with improved stability for microfluidics. *Sensors and Actuators B: Chemical,* 114**,** 239-247.

[33] National Centre for Replacement Refinement & Reduction of Animal Research, 2017, The 3Rs, https://www.nc3rs.org.uk/the-3rs